ISSN Print : 2320-2084, Online : 2321-2950

INTERNATIONAL JOURNAL OF ELECTRICAL, ELECTRONICS AND DATA COMMUNICATION (IJEEDC)

VOLUME NO. 11

ISSUE NO. 2

MAY - AUGUST 2023

ISSN Print : 2320-2084, Online : 2321-2950

International Journal of Electrical, Electronics and Data Communication (IJEEDC)

Aim & Scope

International Journal of Electrical, Electronics and Data Communication (IJEEDC) is having eISSN: 2320-2084 , pISSN:2321-2950, Peer reviewed, Open Access, Indexed and monthly International Journal, being published since year 2013.

IJEEDC is an academic highly reputed, online, open access, peer reviewed international journal. It aims to publish original, theoretical and practical advances in Computer Electrical, Electronics and Communication Engineering and all interdisciplinary streams of Engineering Sciences. All submitted papers will be reviewed by the board of committee of IJEEDC.

Goals Our goals are to promote the co-operation between the professionals in various fields of the Engineering and management to cultivate an environment for the advance and development of the technology. Our objective includes

- Promoting the interactions between the Electrical, Electronics and Communication Engineering
- Advancing the application of engineering techniques from the academics to the industry.
- Facilitating the exchange of information and ideas among the engineers, Scientists, Researchers and academicians easily.

Original ideas may be discussed in advance with the Editor (mail: info.ijeedc@gmail.com), to clear the ground for a draft submission. All papers are then peer-reviewed by relevant experts and feedback is given whether or not a paper is accepted or returned for further work. The Editor's policy is to try and accommodate contributions of all sizes above the minimum threshold where length is dictated by the needs of the subject matter.

IJEEDC publishes both theoretical and experimental high-quality papers of permanent interest, In addition to peer-reviewed original research papers, the Editorial Board welcomes original research reports, state-of-the-art reviews and communications in the broadly defined field of Electronics, Electrical Engineering and Data Communication.

The Journal can be found from the official URL www.ijeedc.iraj.in

ISSN Print : 2320-2084, Online : 2321-2950

ISSN Print : 2320-2084, Online : 2321-2950

ISSN Print : 2320-2084, Online : 2321-2950

International Journal of Electrical, Electronics and Data Communication (IJEEDC)

(Volume No. 11, Issue No. 2, May - August 2023)

Contents

ISSN Print : 2320-2084, Online : 2321-2950

A Numerical Study on Aerodynamic Energy Harvest for Electric Vehicle A Concept to Extend Driving Range

[1] Alemayehu W. Huluka, [2] Chul- Ho Kim
[1]Department of Automotive Engineering, Graduate School, Seoul National University of Science & Technology, 232 Gongneung-ro,N owon-gu, Seoul 01811, Korea
[2]Department of Mechanical & Automotive Engineering, Seoul National University of Science & Technology, 232 Gongneung-ro, Nowon-gu, Seoul 01811, Korea
E-mail: [1]alemayehu@seoultech.ac.kr, [2]profchkim@seoultech.ac.kr

ABSTRACT

Energy efficiency of a road vehicle is highly attributed to its aerodynamic performance. Over some past decades, several improvement has been made and reduced significantly the aerodynamic drag; but, beyond the current achievement, improvement become difficult and challenging for car industry and professionals working in the area. In this regard, this paper focuses on new approach to further find aerodynamic performance improvement particularly for electric vehicles. Therefore, a preliminary numerical study on ducting and concept of energy harvesting from aerodynamic resistance is introduced in this paper. In this numerical study, ducted and slightly modified Ahmed model is used to study aerodynamic characteristics of ducted models and how ducting would contribute to the reduction of energy consumption due to aerodynamic resistance. Furthermore, energy harvesting concept is also introduced as an alternative to improve energy efficiency. Three-dimensional, incompressible, and steady flow governing equations were solved by CFD code (PHOENICS ver.2018) with extended turbulent model proposed by Chen-Kim (1987). From the study, it was found that the total drag was reduced over 15% on the opened front body than the closed one and the kinetic energy harvested in the flow duct is about 15% of the energy consumed due to aerodynamic resistance with M4 model compared to the original blocked model at higher speeds.

Keywords - Vehicle Aerodynamics, Aerodynamic Drag, Ahmedbody, Drag Reduction, Energy Harves

I. INTRODUCTION

Energy efficient vehicles are required to meet future emission and fuel consumption requirements. Environmental issues and public health security concerns have forced car industries and the public to look for alternatives to petroleum based means of transportation. In recent decades, the research and development activities related to transportation have emphasized the development of high-efficiency, clean and safe transportation. Electric vehicles, hybrid vehicles and fuel cell vehicles have been typically proposed to replace conventional vehicles in the future [1], [2].

Currently attention given to electric vehicle development is motivating and it is deemed to be a future car as it is energy efficient, no direct carbon emission, and low noise pollution. On the other hand, the limited driving range per charge is the challenge of current electric vehicles due to low energy density of the battery. To improve the driving range, the first thing which comes to once mind is obviously improving the battery technology. The second alternative is reducing the energy consumption of the moving vehicle that would contribute to increased driving range. In this regard, aerodynamic resistance is the one which have a big share. Therefore, identifying the energy consumption attributes of the moving vehicle and conducting a research on how to reduce consumption of energy would enhance the driving range of the vehicle. The largest portion of power driving the vehicle is consumed to overcome the air resistance [2], [3], [4], [5]. Aerodynamic resistance force typically accounts for 65% of the total resistance for medium sized car at 100 km/hr [2], [4], [5], [6]. Hence, reducing drag force contributes significantly to the energy efficiency of battery electric vehicles [7], [8].

The idea under consideration is harvesting energy from the air resistance without affecting the base drag. As the vehicle is moving in a sea of air, the kinetic energy of the fluid relative to the vehicle is significant particularly at higher vehicle speed. As a first step for a feasibility study, ducting and its aerodynamic effect on a moving vehicle is discussed using simple body. A numerical simulation was made as a preliminary study to either reduce or use aerodynamic resistance of road vehicle.

II. ANALYTICAL THEORY

Theoretical background on road-load power of a moving vehicle, ducting and energy harvesting concept from the aerodynamic resistance is described here in short.

A. Road Load Power and Aerodynamic Drag

The total power required to overcome resistance forces for an electric vehicle cruising at a speed V, can be expressed as:

$$P_{batt} = \frac{1}{\eta_t \eta_m}\left(M_v g f_r V \cos\theta + \frac{1}{2}\rho_a C_D A_f V^3 + M_v g V \sin\theta + M_v \delta V \frac{dV}{dt} \right) \quad (1)$$

The terms in the bracket represent rolling resistance, aerodynamic resistance, grade resistance and inertial resistance to the vehicle motion from left to right respectively. In a high speed driving situation, the power required to overcome the aerodynamic resistance is extremely significant consuming energy to keep its speed. This force is a function of the frontal projected area of the vehicle, drag coefficient and the speed of the vehicle.

$$F_D = fun\ (C_D,\ A_f,\ V,\ \rho_a) \quad (2)$$

Therefore, the drag force is expressed as

$$F_D = C_D \frac{1}{2}\rho_a V^2 A_f \quad (3)$$

Two main components of the drag force are pressure and skin friction force. Aerodynamic resistance of a ground vehicle is dominated by pressure drag whilst skin-friction drag is dominant on aircraft and marine ship[9], [10], [11].

B. Ducting

The frontal area of internal combustion engine powered vehicles is opened with the meshed grill to induct incoming air into the engine room for engine cooling. To the contrary the frontal panel of electric vehicles is closed by design and made up of single panel (fig.1). But the closed frontal panel of electric vehicle would have considerable effect on the increment of aerodynamic resistance of the vehicle .

Fig. 1 Comparison of the front panel shape of two type of sedans
Source [12]

Ducting is not common in ground vehicle as a drag reduction technology. Here in this paper a deliberate duct for either drag reduction or energy harvesting system is made for feasibility study. This kind of approach is believed to be applicable in electric vehicles as mostly their front panel is closed by design and the engine compartment is used as a luggage compartment instead.

C. Aerodynamic Energy Harvest

.When a vehicle moves at higher speed, serious air resistance which is called as drag exerts on the moving vehicle due to the relative wind. If this opposing aerodynamic force acting on a vehicle body due to the momentum loss is ceased by any means, two very positive effects will be expected; fuel savings and emission reduction. If the momentum energy can be recovered, energy efficiency of road vehicle will increase. The energy harvesting concept can be modeled with a radial type power turbine as shown in fig 2.

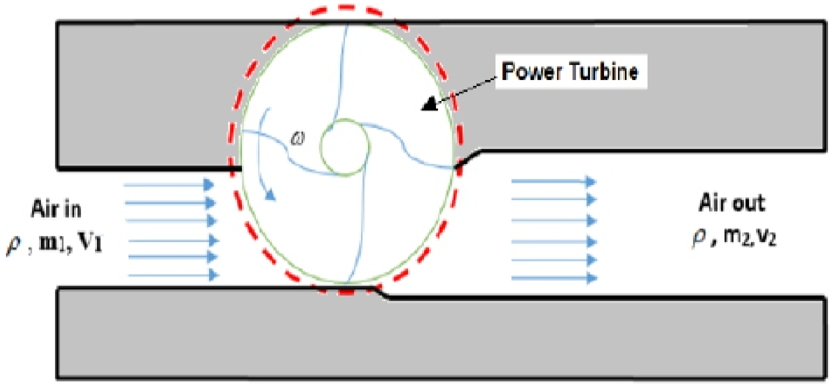

Fig. 2 Schematic drawing of the wind energy harvesting system in an air duct

General conservation of momentum for this model can be stated as the linear momentum equation and it is equal to external forces acting on the control volume.

$$\sum \vec{F}_{ext.CV} = \frac{\partial}{\partial t} \int_{CV(t)} \vec{V} \rho d\forall + \int_{CS(t)} \vec{V} \rho (\vec{V} . \hat{n}) \mathbf{d}A \qquad (4)$$

The force exerts on the power turbine due to the change in momentum at inlet and outlet will be used to calculate the torque of the turbine (dT = Ft x dr). The torque multiplied by the angular velocity of the turbine will give the power harvested from the aerodynamic resistance.

$$Power = \frac{2\pi NT}{60} \qquad (5)$$

Where N is the rotational speed and T is the torque of the power turbine.

III. DESCRIPTION OF THE TEST MODEL

Ahmed model is used for this fundamental study with some modifications. A (4:1) scale model is used with the dimension 4.176m x 1.556m x 1.152m (L x W x H). Five different models are defined with the different size of the duct as specified in table I.

Model No.	Specification of the model	Area ratio
M0	Base model with no duct	0%
M1	Model with 1,072x160 (W`xH`) mm duct	9.6%
M2	Model with 1,072x240 mm duct	14.4%
M3	Model with 1,072x320 mm duct	19.1%
M4	Model with 1,072x400 mm duct	23.9%
Area Ratio(R_A); $R_A = {}^{A_d}/_{A_f}$ where A_f is the frontal projected area of the model and A_d is the cross-section area of the duct(A_d =H`xW`, H`: duct height and W`: duct width)		

Table I Specifications Of The Model Body

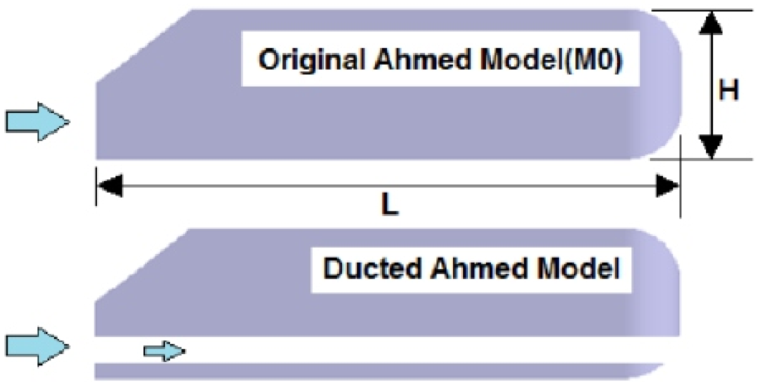

Fig. 3 2-D view of the original (M0)and ducted model body

IV. NUMERICAL SCHEME AND ITS CONDITIONS

In this study, Finite Volume Method (FVM) was used to perform the numerical simulation. The general-purpose CFD code, PHOENICS (ver.2018) was used for a numerical calculation of the turbulent incompressible flow field. 3- dimensional Naiver- Stokes equations were solved with KECHEN turbulent model (Chen-Kim κ-ε model) which is a modified standard κ–κ turbulent model. The turbulent no slip condition near solid boundary was modeled by log law. Chen-Kim κ-ε model believed to improve the dynamic response of the Epsilon equation by introducing an additional time scale and source term. In addition, several of the standard-model coefficients are adjusted so that the model maintains good agreement with experimental data on classical turbulent shear layers [13].

A. Numerical Domain and its Numerical Grid

The numerical domain size is defined as shown in fig 4. Especially 8L is given at the rear side of the model to have a stable convergence on the simulation result. The initial and boundary conditions are defined as given at the table II.

Boundary surface	Boundary & initial conditions
Inlet	Velocity inlet (60, 80, 100, 120km/h)
Outlet	Pressure outlet
Sides and top	No slip wall condition
Ground	moving ground type
Model exterior surface	No slip wall
Duct surface	No slip wall
Flow domain	Quasi-3D flow, Turbulent and incompressible flow

Table 2. Initial And Boundary Conditions

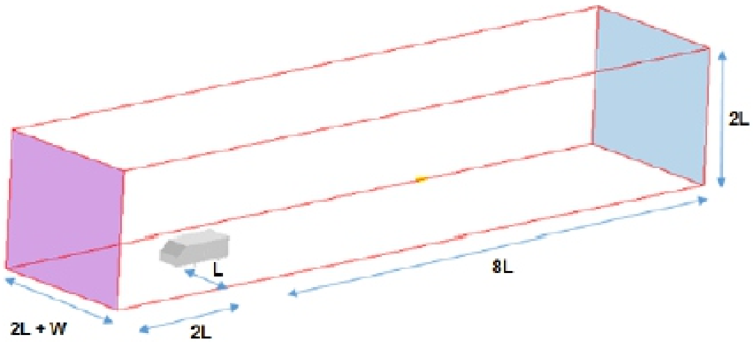

Fig. 4 Numerical domain size for calculation (L=4.176m, W=1.556m)

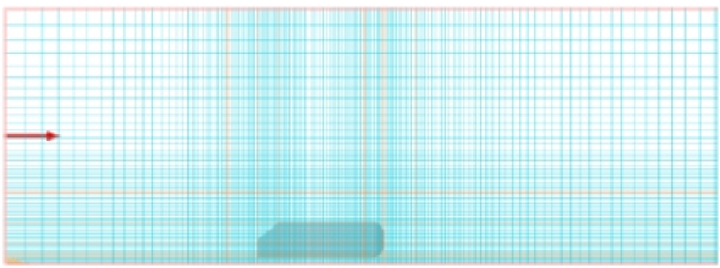

Fig. 5 Optimized grid in the numerical domain (162x94x60)

With the aforementioned set up, numerical simulation has been done to study the duct on drag force, rear flow and related flow property variations. The calculation was conducted at optimized grid distribution with different iterations ranging and very nicely converged with an error cut off less than 0.01%.

B. Governing Equations

For steady incompressible turbulent flows, the flow field is characterized by the conservation laws (since the flow is steady the time derivative component removed). Hence the governing equation for turbulent flow field is written:

1) Continuity equation: $$\frac{\partial U_i}{\partial x_i}+\frac{\partial U_j}{\partial y_i}+\frac{\partial U_k}{\partial z_i}=0 \qquad (5)$$

2) Momentum equation:

$$\frac{\partial}{\partial x_j}(U_iU_j)=-\frac{1}{\rho}\frac{\partial P}{\partial x_i}+\frac{\partial}{\partial x_j}\left[\nu\left(\frac{\partial U_i}{\partial x_j}+\frac{\partial U_j}{\partial x_i}\right)-\overline{u_iu_j}\right]-g_i \qquad (6)$$

Where, $-\overline{u_iu_j}=\nu_t\left(\frac{\partial U_i}{\partial x_j}+\frac{\partial U_j}{\partial x_I}\right)-\frac{2}{3}k\delta_{ij}$,

$\delta_{ij}=1 \;\; if\; i=j \;\; and \;\; \delta_{ij}=0 \;\; if\; i\neq j$

3) Extended κ-ε closure turbulent model (KECHEN)

- Turbulent kinetic energy equation

$$\frac{\partial}{\partial x_i}(U_jk)=\frac{\partial}{\partial x_i}\left[\left(\nu+\frac{\nu_t}{\sigma_k}\right)\frac{\partial k}{\partial x_j}\right]+G-\varepsilon \qquad (7)$$

$G=-\overline{u_iu_j}\frac{\partial U_i}{\partial x_j}$ (production rate due to deformation) [14].[15].

$\nu_t=C_\mu\frac{k^2}{\varepsilon}$, $C_\mu=0.09$

- Energy dissipation equation

$$\frac{\partial}{\partial x_i}(U_j\varepsilon)=\frac{\partial}{\partial x_i}\left[\left(\nu+\frac{\nu_t}{\sigma_\varepsilon}\right)\frac{\partial\varepsilon}{\partial x_j}\right]+\frac{\varepsilon}{k}(C_{\varepsilon1}G)-C_{\varepsilon2}\frac{\varepsilon^2}{k})+C_{\varepsilon3}f_1\frac{P_k^2}{K} \qquad (8)$$

Where, ($C_\mu=0.09$, $C_{\varepsilon1}=1.15$, $C_{\varepsilon2}=1.9$, $C_{\varepsilon3}=0.25$

$\sigma_k=0.75$, $\sigma_\varepsilon=1.15$)

V. RESULTS AND DISCUSSION

The force distribution over the model is evaluated under „integrated forces" indicating pressure force and friction forces. Based on this integrated force results, evaluation of the duct flow effect on each and every side is made possible. Special attention is given to the drag force being contributed from pressure force and skin friction force. The frontal pressure force and rear side drag force due to strong and counter rotating trailing vortex.

A. Aerodynamic Flow Characteristics of the Model

Aero dynamic characteristics of the flow around the model is demonstrated using the static pressure contour plot as depicted in fig.6. The pressure distribution at front and rear of the un ducted and ducted model are different due to the duct effect. M1 with the opened front panel has lower the front stagnation pressure than the fully blocked body and higher the rear induced pressure due to the flow wake resulting in reduced pressure drag.

Fig. 6 Pressure distribution on M0 and M1 at 100km/h

B. Pressure Drag Force

Effect of the opened front panel on pressure drag force is evaluated in detail. The total pressure drag curve versus models with different duct size is shown in the fig. 7.

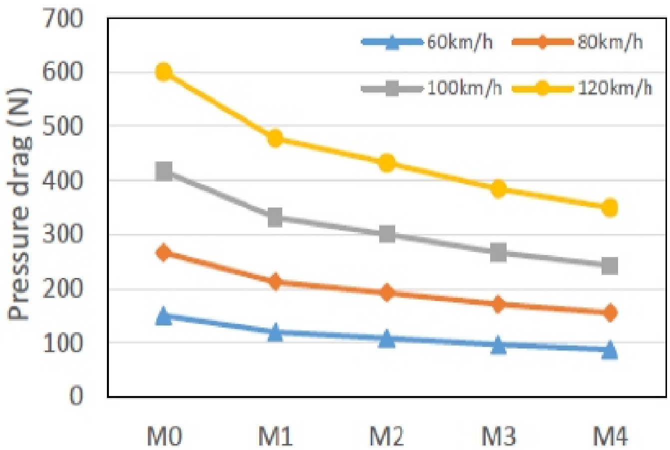

Fig. 7 Variation of the pressure drag with the duct size at different speed

The highest pressure force is observed on the model M0. As the duct size increases the pressure force magnitude is decreasing. quantitatively, for M1 model at a speed of 80km/h about 20.5% reduction of total pressure drag in reference to the base model. This shows that the duct has a very significant effect on a pressure drag reduction of the bluff body under consideration.

C. Skin Friction Drag

The friction drag generated due to boundary layer effect and turbulent flow is relatively small. During this study, contrary to the pressure force, the friction drag force of the ducted models revealed an increasing trend as duct size increases. The model with no duct (base model) experienced the smallest friction drag. This could be due to increased surface area and flow separation created in each inner sharp corners of the duct.

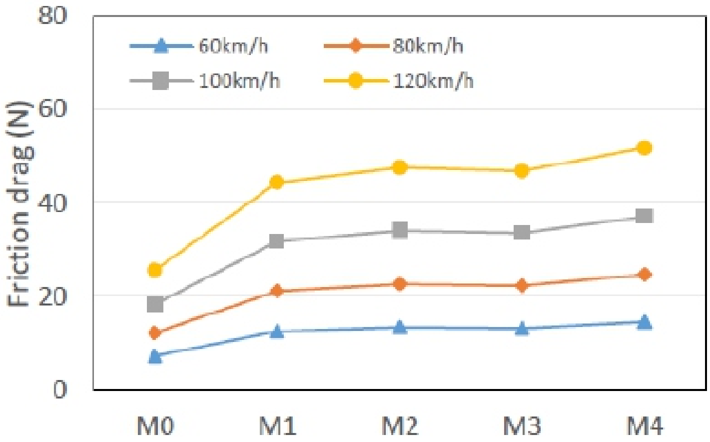

Fig. 8 Variation of fiction drag with the duct size at different speed

Considering one of the ducted models with smallest duct size (M1) at speed of 100km/h a net total drag reduction of about 16.3% is observed quantitatively. The pressure drag force is reduced by 19.5% while the skin friction drag is increased by 3.2% of the total drag. As the duct size increases, the friction force increases as shown in fig. 8. This can be considered as side effect of ducting as far as drag reduction is concerned while the pressure force which is the dominant drag force in ground vehicle exhibit a decreasing trend. Since the contribution of skin friction to the total drag is very low, its increase with duct size didn‟t affect much the decreasing trend of the total drag force

D. Drag Coefficient

The coefficient of drag of the models also showed a reduction trend even though coefficient of drag is directly proportional to drag force and inversely proportional to reference area (Af), reduction of both area and drag force by ducting does not assure a reduction in CD. The relative change rate of area and change rate of drag force is a determining factor for reduction of the CD of ducted model. As shown in fig. 9, about 15.3% of CD was reduced in Model 4 body comparing to the original Ahmed model(M0) in speed range. It should be noticed that an opened front panel on a moving body should have energy saving effect than the closed one and will contribute to driving range extension.

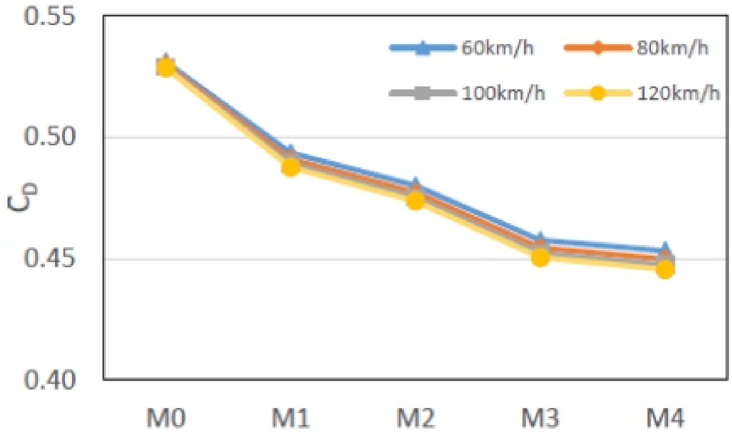

Fig. 9 Variation of drag coefficient with the duct size at different speed

E. Aerodynamic Energy The velocity profile just before the entry, at the entry, inside duct, at the exit and just after the exit of the duct gives some insight about the flow dynamics and energy level at the duct. To have a big picture of the flow domain along duct a wider range velocity profile is plotted as dipicted on fig. 10. The profile is captured with in a 10m long distance in the doman passing through the middle of the duct length to see the pattern of the flow speed. At about 3m in front of the duct, the velocity assumes a free stream velocity (27.78m/s). This velocity declines as it approaches the object (model) front side and sharply drop to about 65% of the free stream velocity near the entry edge of the duct and then raise back to about 86% at the entry. Just after entry it slightly decelerates until it attain smooth flow inside the duct where it gradually accelerate. At the exit, it drastically decelerate again as it is exposed to a chaotic tubulent flow at the rear of the object until it mix with and maintain the outside rear flow structure about 3m behind the rear end.

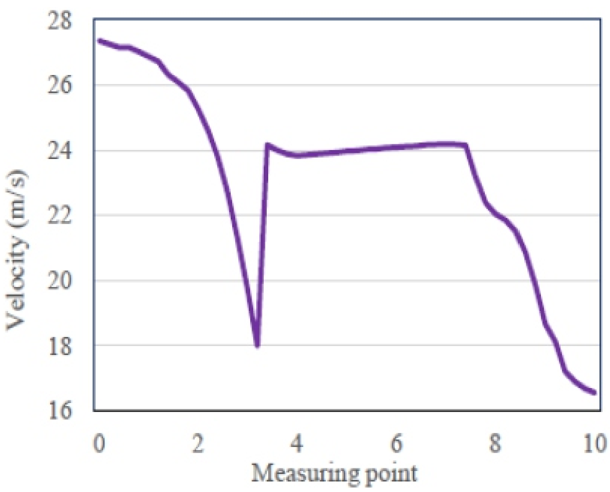

Fig. 10 Longitudinal velocity distribution in the model duct center of M1

Hadn"t been a duct, the kinetic energy of the whole bulk flow is stagnated at the front exerting a resistance to the object. But now it can be seen in the profile plot that some amount of the flow kinetics is maintained and channeled to the rear through duct reducing the aero dynamic resistance. This kinetic energy of the air can be harvested using the principle discussed in section II subsection C of this article. Considering the typical scenario power to be harvested is estimated for model M1.The calculation is performed with the following assumption. Air density is uniform throughout the duct. As the flow is guided to the turbine by duct, the turbine converts major portion of the kinetic energy in the air to mechanical energy turning the generator. Turbine is directly connected to the alternator mechanically. Therefore, the potential aerodynamic kinetic energy by the air flowing through a duct is estimated by,

$$\text{Kinetic Energy} = \frac{1}{2}\rho A \overline{U}^3$$

The average air velocity $\overline{U}$ inside the duct is expressed as,

$$U = \frac{\iint V_n dA}{A}$$

The available power harvested could be calculated as,

$$P_{available} = \frac{1}{2}\rho A \overline{U}^3 \eta_T \eta_g \qquad (9)$$

Table III shows the electric energy harvested by the kinetic energy of air passing through the duct of the model(M4) under the reasonable assumptions.

Vehicle speed (km/h)	Averaged air velocity in the duct (m/s)	Turbine efficiency (%)	Generator efficiency (%)	Usable power (watt)
60	13.60	85%	88%	192
80	18.18	85%	88%	458
100	22.79	85%	88%	903
120	27.39	85%	88%	1,567
Power turbine and generator efficiency (assumed)				

Table iii. Estimation of The Electric Power Harvested In M4

As shown in table III, the harvested electric energy proportionally increases with the model speed. As the speed reaches to 120km/h, the power harvested is up to 1.567kW. With Model M4, the usable energy harvested is calculated to be over 15% of the energy consumed due to aerodynamic resistance of the model without duct at higher speeds. For the estimation of total driving range extension with this air duct installed at the front side of the model vehicle, both the aerodynamic drag reduction and the electric energy harvested should be considered. In the following analytical study the detailed theoretical approach and method will be discussed.

VI. CONCLUSION AND FUTURE WORK

In this numerical study, it was found that the air flow duct installed at the frontal surface of the model vehicle show the positive effects on the total drag force. It was also confirmed that pressure drag force accounts for more than 90% of the total drag. The pressure drag shows a decreasing trend as duct inlet size increases but the skin friction drag increases with the duct inlet size. Velocity profiles indicate the ducted flow characteristics particularly the fluid acceleration and deceleration before, at the duct entry, exit, and after exit respectively. The level of kinetic energy preserved through ducting is also observed. The electric energy harvested from this kinetic energy of the flow in the duct would contribute to driving range extension of electric vehicle. Effect of ducting on the stability of the model, feasibility of energy harvesting through ducting and rear flow control for better duct flow acceleration is part of the future work.

REFERENCE

[1] E. Mehrdad Ehsani, Yimin Gao, Modern Electric, Hybrid Electric and Fuel Cell Vehicles, Second Edi. CRC Press, 2010.

[2] C. Kim, "A Streamlined Design of a High-Speed Coach for Fuel Savings and Reduction of Carbon Dioxide," Int. J. Automot. Eng., vol. 2, pp. 101–107, 2011.

[3] S. Nalanagula and G. T. Varadharajan, "Aerodynamics Drag Reductions Methodology for the Commercial Vehicles Using Computational Fluid Dynamics," SAE Tech. Pap. Ser., vol. 1, 2016.

[4] R. C. McCallen et al., "Doe''s effort to reduce truck aerodynamic drag - joint experiments and computations lead to smart design," in 34th AIAA Fluid Dynamics Conference and Exhibit, 2004, no. July, pp. 1–16.

[5] R. McCallen et al., "Progress in Reducing Aerodynamic Drag for Higher Efficiency of Heavy Duty Trucks (Class 7-8)," SAE Tech. Pap. Ser., vol. 1, no. 724, 2010.

[6] A. Altinisik, O. Yemenici, and H. Umur, "Aerodynamic Analysis of a Passenger Car at Yaw Angle and Two-Vehicle Platoon," J. Fluids Eng., vol. 137, no. 12, p. 121107, 2015.

[7] W. Hucho and G. Sovran, Aerodynamics of Road Vehicles, vol. 25, no. 1. 2003.

[8] T. V. Johnson, "Review of Vehicular Emissions Trends," SAE Int. J. Engines, vol. 8, no. 3, pp. 2015-01–0993, 2015.

[9] R. M. Wood, "Impact of Advanced Aerodynamic Technology on Transportation Energy Consumption," SAE World Congr., vol. 2004, no. 724, pp. 1–21, 2004.

[10] S. A. E. International and S. A. E. Transactions, "Some Salient Features of the Time -Averaged Ground," vol. 93, no. 1984, pp. 473–503, 2018.

[11] D. K. Kalyan and A. R. Paul, "Computational Study of Flow around a Simplified 2D Ahmed Body," Int. J. Eng. Sci. Innov. Technol., vol. 2, no. 3, pp. 148–153, 2013.

[12] www.hyundai.com, Posted on Oct. 21, 2017.

[13] Y.-S.Chen and S.-W. Kim, "Computation of Turbulent Flows Using an Extended K-Epsilon Turbulence Closure Interim Report," Alabama, 1987.

[14] H. Tennekes, A First Course in Turbulence. Massachusetts: The MIT Press, 1972.

[15] G. Recktenwald, "The k− Turbulence Model." pp. 1–20, 2009.

[16] J. Banks, "Turbulence Modeling in PHOENICS," 2007. [Online]. Available: http://www.cham.co.uk/phoenics/d_polis/d_enc/turmod/enc_t 342.htm.

ABBREVIATIONS AND SYMBOLS

F_D: drag force

V: vehicle speed

M_v: Mass of the vehicle

g: gravity

f_r: rolling resistance coefficient

θ: slope or grade

δ: mass factor

P_{batt}: battery power required to drive the vehicle

η_T: turbine efficiency

η_g: generator efficiency

η_t: power turbine efficiency

η_m: traction motor efficiency

A_f: frontal projected area of test models

C_D: drag coefficient

ρ_a: air density

k: turbulent kinetic energy

ε: energy dissipation rate

V_l & V_t: laminar and turbulent kinematic viscosities

P_k: is the volumetric production rate of kinetic energy by shear forces.

σ_k, σ_ε: Pradtl number connected to diffusivity of K and ε to eddy viscosity

f_1: is the Lam-Bremhorst [1981] damping function which tends to unity at high turbulence Reynolds numbers[16].

δ_b: boundary layer thickness

L: Model length (characteristic length)

F_{ext}: external force

dT: differential Torque

$\overline{U}$: averaged air speed in the duct

Design and Develop Smart Smoke and Fire Detector on Raspberry Pi 3 Connecting Arduino

[1] **Sutthisak Pongcharoen,** [2] **Paniti Netinant**

[1,2]Rangsit University, Master of Science in Information Technology Program, Graduate School, Pathumthani, Thailand E-mail: [1]sutthisak.pong@gmail.com, [2]paniti.n@rsu.ac.th

A B S T R A C T

In the present days, the real-time resident security is very important for every location. Whether it is used to protect various events. When serious events occur it can be alert, collecting various incidents and analysis of potential issues to use security planning and to protect future incidents. Therefore, Internet of Things (IOT) can be used for a security system to solve issues with inspection of various incidents as a preliminary notification before serious incidents occur such as ventilation issues, fire or pollution that affect people living inside the building. Our design makes a smart smoke and fire detector more efficient by using smoke and heat sensors from Arduino and Raspberry Pi 3 for monitoring notification, storing data, and displaying to prevent incidents in the future and will be able to use the collected data to analyze and plan for future issues. The aim of this research will design a better detector of fire and pollution for resident or any building by using Raspberry Pi 3, Arduino, and Sensors.

Keywords - Smart Smoke Detector, Smart Fire Detector, Internet of Things, Home Security, and Arduino.

I. INTRODUCTION

In recent years, the Internet of Things (IOT) technology has been an important part in developing diverse information systems and being able to use it more conveniently. For example used in industrial plants to control machinery. Use for medical purposes to track the patient's condition. Used for the development of a non-toxic vegetable growing system to check soil quality. Or even to identify the person to be used to track the status of the person. Therefore, if those technologies are used for security especially with accommodations for use in investigating undesirable incidents to prevent various losses. When we go out to work, we are not able to recognize about our housing status. If designing those systems was developed by a low-cost device that can be used more function and varied range if using these technologies to help with security. So developing from Raspberry and Arduino. Devices that are not very expensive but can be designed in many systems such as toxic smoke detection systems Temperature monitoring system or fire alarm system and apply these technologies to the internet network unlimited connections. Able to alert in the event of a warning or notifications through various applications and still have those data stored as databases for reference and can be analyzed to plan the prevention of incidents that may occur and can also be further developed into an intelligent home system.

In which the operation of a traditional smoke detector or fire detector can be used only within a limited scope and covering certain areas. Which causes restrictions on usage and is not able to notify users when they are outside of the premises or outside their residences. The operation principle of these machines will detect smoke as has been configured and the alert will sound within itself and will be don't sent information to elsewhere. But, SSFD system can detect smoke, temperature and flame. It can use voice notifications via buzzer, notification via application. Other than, this device can store data and send to central database. Summarize inspection results, alerts or notifications and user can access the device through the Internet from anywhere.

The Intelligent Home system is therefore worthwhile to use. Used to detect faults from installed sensors. For example temperature sensors, humidity sensors, infrared sensors, smoke sensors and buzzer for offline alarms. The operation of these sensors will send information to the Arduino NodeMCU for process, checking errors and find issues. Buzzer will alert immediately even if there is no internet signal. But, If connection online. All data can be stored in a database processed by Raspberry Pi 3 and if suspicious data is entered. The system will notify you through the application and it can to check data history, so the system can be used in a variety of ways and helps to increase the potential for greater security.

II. LITERATURE SURVEY

In every location around the world, security issues are important to everyone's life. Especially the maintenance of housing safety or the detection of abnormalities that may affect the health of each person. Designing a system of devices that can inspect various things around is important. And the fire problem is important for everyone. We don't know when that will happen.

If use this system. It can monitor a place or a location and accurately locate where a fire has broken out so that immediate action can be taken to mitigate losses and casualties. As a solution to this problem, we propose a network of Internet of thing (IOT) devices which continually monitor for fire and alert a central hub if there is a fire about the occurrence and its location. From there on, this information is sent to the concerned people and authorities so that preventive measures can be implemented. For this, we have designed an MQTT network where a Raspberry Pi acts as the MQTT Broker and a distributed group of NodeMCUs attached with smoke and temperature sensors act as a sensor network to relay information to the Raspberry Pi [6].

A. SSFD System

Kevin Ashton, father of the Internet of Things in 1999 while doing research at the university. Massachusetts Institute of Technology (MIT). He was invited to give a lecture to Procter & Gamble (P&G). He proposed a project called Auto-ID Center, built on RFID technology that was at the time considered the world standard for Kevin said that the sensors can enable them to talk to each other through his Auto-ID system. By describing P&G at that time, Kevin used the term Internet of Things in the slide. His first lecture by Kevin term is defined at the time that any electronic device that can communicate with each other, it is. "Internet-like" or simply speaking, electronic devices that communicate the same way with the internet. The term "Things" is a term used to represent those electronic devices. Later in the year 2000, many electronic devices were produced and distributed throughout the world. So, started using the word Smart, which is Smart Device, Smart Grid, Smart Home, Smart Network, Smart Intelligent Transportation. All of these are embedded with RFID Sensors like adding ID and brain, allowing them to connect to the internet. Which those connections are, therefore, an idea that those devices can also communicate with each other by using sensors to communicate with each other This means that apart from the Smart Device will be able to connect to the internet Can also connect to other devices as well.

The design of the SSFD system to operate at full efficiency Therefore, both types of Internet of Things (IOT) devices are combined between the Raspberry Pi 3 and the Arduino NodeMCU. The function is divided into parts. The first part is for initial inspection and processing, include the Arduino NodeMCU has introduced 3 types of sensors to help monitor various events. The sensor (1) MQ2 Smoke detector Sensor is to check the toxic smoke signal and send the value to be received at NodeMCU. (2) DHT22 Temperature Sensor is to check the device in the air and humidity change. All received data will be sent to NodeMCU for further processing. (3) Flame sensor infrared detects the light that may be the origin of the flames that may rise before other sensors capture. Signal It will work together on all 3 types of sensors through NodeMCU processing which will be monitored all the time, which, if any unwanted events occur, the device will alert itself within Buzzer. It is a preliminary notification in order to stimulate the residents to be alert and observe the mistakes that have occurred. The second part, after NodeMCU has processed the values. All data will be sent to the Raspberry Pi 3 that has the database installed. The time data will be recorded from NodeMCU and users can retrieve those data back through the specified application.

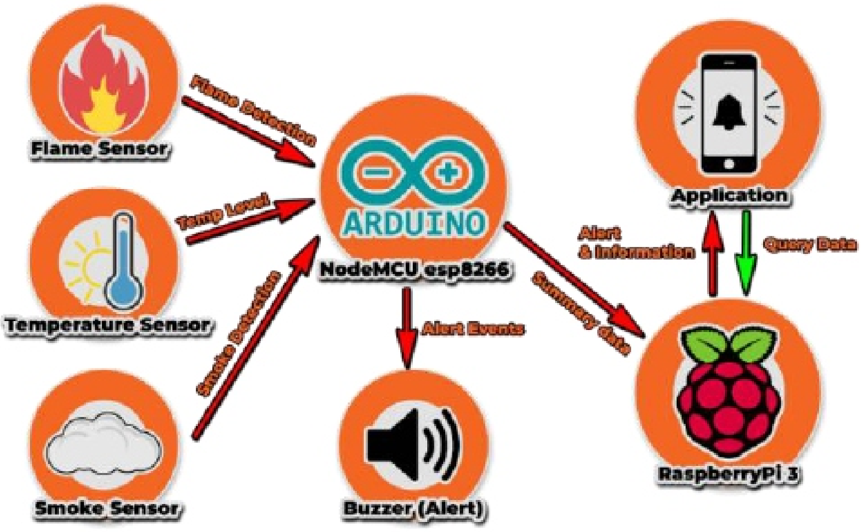

Figure 1. The SSFD Architecture

B. Raspberry PI

The Raspberry PI 3 model B is a tiny and low weight, it supports many functions of computer, that can connection to monitor and USB support devices. It has Broadcom BCM2837 System on Chip (SoC). It has a CPU (central processing unit) which is ARM compatible, and also a video Core IV GPU (graphics processing unit). It has a single processor which runs at 1.2GHz and includes a RAM of 1GB.

Storage can be included in the form of a micro SD card for which a slot has been provided. The Raspberry Pi operates in the open source ecosystem. It runs Linux, and its main supported operating system, Raspbian, is open source and runs a suite of open source software. The Raspberry Pi Foundation contributes to the Linux kernel and various other open source projects as well as releasing much of its own software as open source. And revealing to everyone to learn and use by many languages such as Python or C#. Aside from system development can also use a wide range of multimedia including surfing the web, watching movies, listening to music and working in documents.

Figure 2. Raspberry PI 3 Model B

C. Node MCU

NodeMCU is a platform of Arduino used to help build Internet of Things (IOT) projects including development kit (Board) and Firmware (Software on Board) which is open source. It can be written in Lau language. Easier comes with a Wi-Fi module (ESP8266) which is the key to connecting to the internet and the hardware designed according to the ESP-12 module is one of the most popular choices for many people working with IoT applications because of their small size and cheap price. Due to its compact design, the power consumption is very low. And data processing with 128kB of RAM and 4MB of storage space. With one analog and eight digital GPIO, it is convenient to use a variety of applications that include sensors and actuators. Convenient to use as it is a versatile device and has many documents on the internet. Due to the advantages of memory size and power usage, it has become one of the most selective microcontrollers in operation and design for Smart Home and IOT [10].

Figure 3. Node MCU

D. DHT Sensor

The DHT22 sensor is upgrade from DHT11 sensor. It use sensor model AM2303. This is a low-cost and low-power sensor to measure the temperature and humidity in the atmosphere. DHT22 is support temperature rate -40 to 80 Celsius from the DHT11 support around 0 to 50 Celsius. The DHT sensor is made up of two parts, the capacitive humidity sensor and a thermistor. We can read the data directly without having to do calibrations of any sort for temperature or humidity.

Figure 4. DHT Sensor

E. MQ2 Sensor

MQ2 is a smoke sensor that we use to detect the existence of Combustible gas and smoke, this sensor uses a small heater inside with an electrochemical sensor, it's sensitive to toxic fumes in the air and can be used to detect various gases. The operation of the sensor sends analog data to the device. Which is connected by showing a higher smoke charge Higher is the value that can be read from the smoke.

The sensor therefore makes interpretation easier. With wide detection High sensitivity range and fast response time are easy. Design sensor that has a long and stable service life.

Figure 5. MQ2 Sensor

F. Flame Sensor

Flame Sensor detector flames using Infrared sensor outputs analog signals. The sensitivity can be adjusted at the volume on the module. Flame sensor most sensitive to ordinary light is also a reaction, generally used as fire alarm and other purposes. A small panel output interface can be directly connected with the microcontroller IO port. The sensor and the flame must maintain a certain distance (more distance 80cm), so as not to damage the sensor.

Figure 6. Flame Sensor

G. Buzzer

The device indicating sound is used for alerting various events. There are 2 wires. Red wire is connected to the power source (Power Input). Black wire connect to ground (GND). The sound level is at the voltage of the connected equipment. If the voltage is high, the sound will be loud. If the voltage is low, the sound will be low.

Figure 7. Buzzer

III. HARDWARE SETUP

The hardware setup consists of the first part, Raspberry Pi acting as the main database, which is responsible for storing data sent from NodeMCU in the form specified, the second part consists of NodeMCU connected to the sensor for monitoring various events, including 3 Sensors MQ2 Sensor, DHT22 Sensor, Flame Sensor and the buzzer is also connected for voice alerts or offline alerts.

IV. SOFTWARE SETUP

The software usage is divided into 3 parts.

1. Raspberry Pi has introduced MQTT Broker to control the display on Application by running on Raspbian system.
2. NodeMCU has introduced Sketch program to develop code for writing commands on the device.
3. Sensors have installed library to support the operation of sensors including DHT22, Mq2.

A. MQTT Broker on Raspberry Pi 3

MQTT broker is a protocol designed for M2M connection. It supports the connection between devices and devices for IOT technology. In designing this system, we have selected the protocol to support the operation of each device which is MQTT-Mosquitto Install and run Mosquitto on Raspberry PI 3 inside the operating Raspbian system.

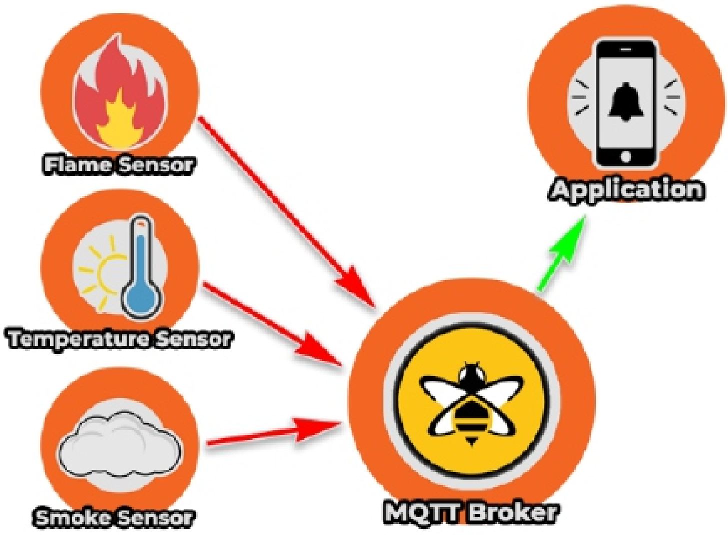

Figure 8. MQTT Broker

B. Sketch on NodeMCU

Sketch is a program used to write a set of instructions on the board Arduino. Which is one of the most popular programs. It call another name is the Arduino IDE (Integrated Development Environment). Due to being easy to use and this program that is freely available and free of charge. For this project, it was designed to support many types of connected signals, including MQ2 sensors, DHT22 sensors, and NodeMCU flame sensors that receive analog signals. It can will develop codes for conversion into easy-to-understand values and displayed on screen for everyone to understand .

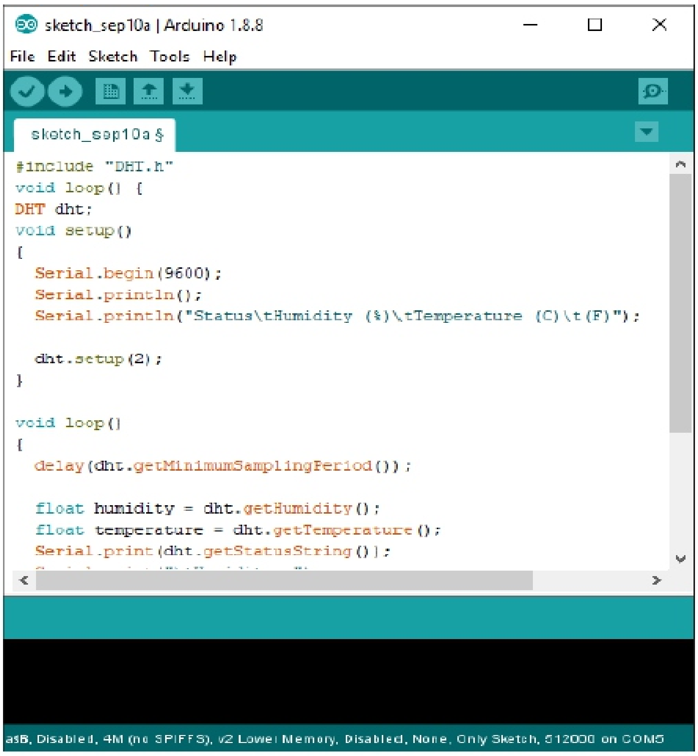

Figure 9. Sketch decode form any sensors.

C. Library of NodeMCU Sensors

Library is a set of codes that have been written and recorded into a file on a computer. For easy to use on writing a large amount of code. Increase the efficiency of the reordering of the code to be shorter and more compact.

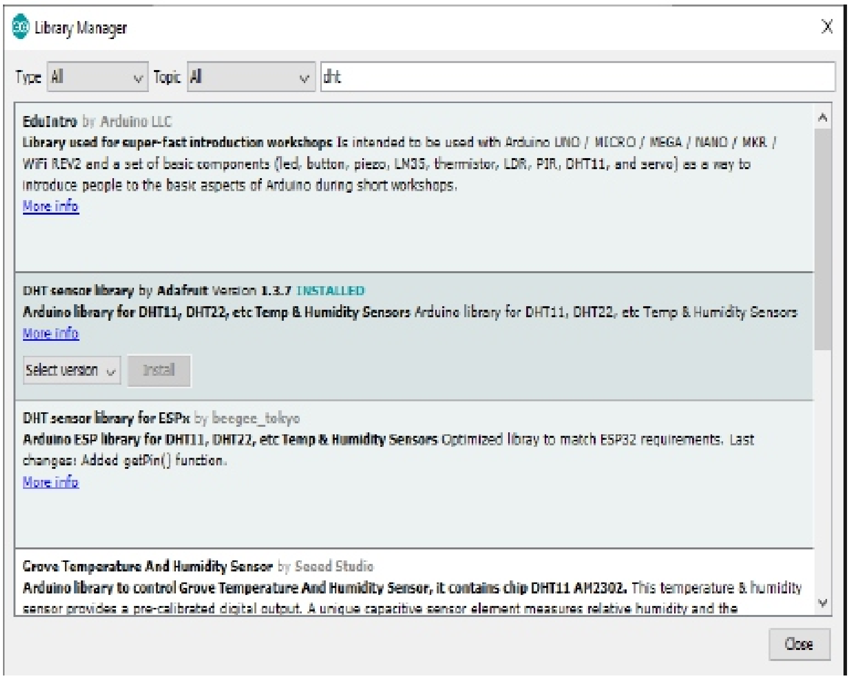

Figure 10. Library of NodeMCU Sensors

V. CONCLUSION

This project demonstrates the use of IOT devices for home security purposes. By bringing different types of sensors to connect and work together for the highest efficiency. The flexibility of the connection can be made into a network of IOT systems by connecting through a Wi-Fi network together. And planning the lowest cost design and without additional costs. This system can be applied to other IOT systems to increase work efficiency and a variety of functions. Therefore it is truly a design of the smart house.

REFERENCE

[1] Md Saifudaullah Bin Bahrudin, Rosni Abu Kassim, Norlida Buniyamin, et al. (2013), "Development of Fire Alarm System using Raspberry Pi and Arduino Uno", International Conference on Electrical, Electronics and System Engineering (ICEESE) 2013

[2] D. Pavithra, Ranjith Balakrishnan, et al. (2015), "IoT based monitoring and control system for home automation", Global Conference on Communication Technologies (GCCT) 2015

[3] Muhammad Noman Aqeel Khan, Talha Tanveer, Kiran Khurshid, Hassan Zaki, Syed Sajjad Imam Zaidi, et al. (2019), "Fire Detection System using Raspberry Pi", International Conference on Information Science and Communication Technology (ICISCT) 2019

[4] Ravi K Kodali, Aditya Valdas, et al. (2018), "MQTT Implementation of IoT based Fire Alarm Network", International Conference on Communication, Computing and Internet of Things (IC3IoT) 2018

[5] Meo Vincent C. Caya, Angeline P. Babila, Alyssa Moya M. Bais, Seoi Jin V. Im, Rafael Maramba, et al. (2017), "Air pollution and particulate matter detector using raspberry Pi with IoT based notification", 2017IEEE 9th International Conference on Humanoid, Nanotechnology, Information Technology, Communication and Control, Environment and Management (HNICEM)

[6] Md. Muminur Rahman, Monir Hossen, Md. Taybur Rahama, et al. (2017), "Raspberry Pi as Sensor Node and Hardware of the Internet of Things (Iot) for Smart Home", International Journal of Innovative Research in Electronics and Communications (IJIREC), Volume 4, Issue 1, 2017, PP 12-19

[7] H. K. Merchant, D. D. Ahire, et al. (2017), "Industrial Automation using IoT with Raspberry Pi", International Journal of Computer Applications (0975 – 8887) Volume 168 – No.1, June 2017

[8] Shivani Sharma, Kailash Chand, Deepak Sharma, Paramita Guha , et al. (2018), "Development of an early detection system for fire using Wireless Sensor Networks and Arduino", International Conference on Sustainable Energy, Electronics and Computing Systems (SEEMS) 2018

[9] Suresh S. , Yuthika S. , G.Adithya Vardhini, et al. (2016), "Home based Fire Monitoring and warning system", International Conference on ICT in Business Industry & Government (ICTBIG) 2016

[10] "Nodemcu – an open-source firmware based on esp8266 wifi-soc". From http://nodemcu.com/index en.html/

ISSN Print : 2320-2084, Online : 2321-2950

Development of Rough Terrain Mobile Robot by Self-Position Estimation used Single Marker and Outer Product

[1] Yuki Kurahashi, [2] Hideki Toda
[1,2] Dept. of Electric and Electronic Engineering, University of Toyama Gofuku Campus, 3190 Gofuku, Toyama, 930-8555, Japan E-mail: m1871014@ems.u-toyama.ac.jp

A B S T R A C T

In the present study, a mobile robot control strategy of rough terrain capable of position and direction estimation by a single marker was proposed, and the effect was performed. To realize wheel / caterpillar mobile robot movement on the rough terrain such as house farm, two major problems (1) the precise position estimation and (2) the direction estimation are important before the development of the control theory. Generally, the position / direction have been estimated by the wheel rotation (odometry) and gyro or acceleration sensor's output integration, but there are many problems such as many impacts from the ground and the wheel slipping on the rough ground to the precise estimation. The aim of this study is to develop a method (algorithm) to estimate the mobile robot direction using a single marker placed at the top of the robot by changing the front movement and the target direction movement periodically. The reason using a single marker is that it is difficult to process to find and analyze positions of the many markers attached on the robot in the camera image from a long distance, and the positions of many markers have been unstable by the tilting of the robot, agricultural product's shadow, getting dirty of the body and so on. Our proposed method would be effective in the difficult situation to find or analyze the marker position of the robot surfaces by the reason of camera position and the environment, and it could realize wheels / caterpillar type mobile robot movement on the muddy situation.

Keywords - Odometry,Caterpillar Mobile Robot,Outer Product, Marker.

I. INTRODUCTION

In this paper, a mobile robot control strategy of rough terrain capable of position and direction estimation by a single marker was proposed, and the effect was performed. Current agriculture in Japan has a problem of aging of agricultural workers, and the substitution of agricultural work by robots is becoming increasingly important socially[1]. To realize wheel / caterpillar mobile robot movement on the rough terrain such as house farm, two major problems (1) the precise position estimation and (2) the direction estimation are important before the development of the control theory.

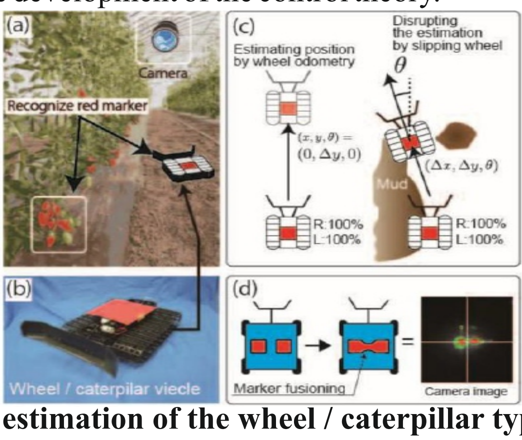

Fig.1 Difficulty of the position estimation of the wheel / caterpillar type mobile robot platform in the rough terrain house farm

Figure 1a shows the major situation of the mobile robot movement environment for application in the house farm. Previously proposed robot application in house farm used multi aluminum / stainless rails on the ground to realize correct position / direction movement of the robot[2], however many costs are necessary for the equipment and the rails become a factor hindering effective use of agricultural ground. Even if the rail is set up on the farm, the problem of measurement and movement of the mobile robot's current position is caused by dirt or slippage on the rail. The need for long-term maintenance has not yet been discussed. As another solution of the mobile robot localization and control, colored markers attached on the mobile robot (ex. Fig. 1b) could be used, and the position would be measured by camera attached on the ceil. But the extracting position of the markers are generally difficult by the reason of mixing with environment colors, marker shape (area) instability, the distance from the camera to the markers, and multi markers geometric position combination problem[3]. To estimate the position and the direction of the robot, two markers are necessary at least in 2D map. But it is not always possible to detect the two markers in the rough terrain field in the house farm by above some reasons, especially a marker fusion is a serious problem (Fig.1d) in this situation. This causes disable robot direction detection. In addition, since the wheel / caterpillar rotations affected by the slip on the dirt (Fig.1c), the position estimation by the wheel / caterpillar rotations (odometry) was failed generally. Our proposed method uses one marker of the mobile robot to improve the detection performance of the robot with the camera on the ceiling, and estimates the direction of the robot with a new two-phase motion control algorithm using the outer product. In this paper, we performed a basic study of position estimation / movement control of a caterpillar mobile robot on rough terrain.

II. PREVIOUS STUDY

Auto-runner[4] is a previously proposed unmanned pesticide spreader in house farm environment. It could realize the pesticide spread by moving the all area on the house railed with metal rail. Since the robot does not estimate its own position, it cannot manage with slippage on the rail, and it is expensive setup. In University of Shimane[5], it represents omnidirectional mobile robot to convey objects in a complicated and narrow environment by using a special wheel called a omni-wheel, it can move in all directions. It have constructed an algorithm that estimate the position and orientation of the mobile robot with high accuracy acceleration and gyro sensors mounted on the robot, and the rotation angle of the driving wheel. Since the wheel usually slipped on the farm, the acceleration and gyro sensor values could not correspond to the real wheel rotation angle information and it is impossible to estimate the correct position and direction.

III. METHOD

A. Experimental Devices and The Setup

Figure2 shows the experimental setup devices, (a) Caterpillar mobile robot (BLIZZARD SR, Kyosyo Corp., 35cm ×30cm ×8cm) attached red marker (0.18m ×0.18m), (b) Setup of the experiment. Camera (640 pixels×480 pixels, view angle 130 deg, 30 fps) was attached on the ceiling, and two markers were used as the robot and target position respectively. The mobile robot was controlled by two channel motor driver, Arduino microcomputer and middle spec PC (AMD A10-7860K, 8GB ram).

B. Control Algorithm

The mobile robot was controlled by two different control strategy in this study. When the center of the gravity of the red markers were measured as $\vec{x}_1$ (robot) and $\vec{x}_2$ (target), the direction of the target was defined $\vec{b}=\vec{x}_2-\vec{x}_1$ (Fig.3a). Normal vector $\vec{a}$ was defined as estimated robot direction, and it was calculated from Method (a) the robot caterpillar rotations and (b) a 300 ms period "forward" movement

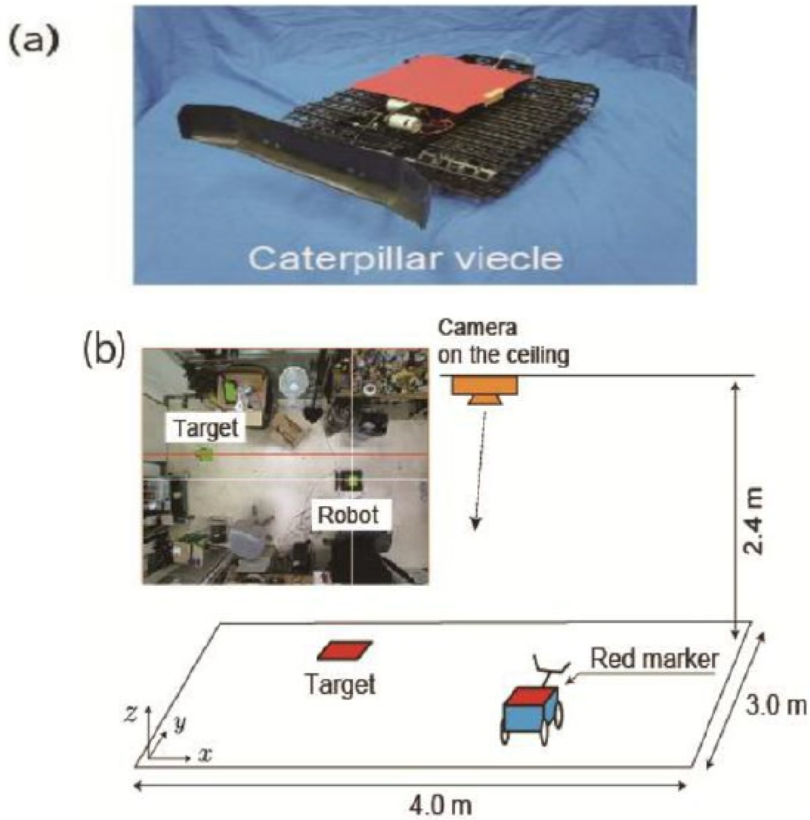

Fig. 2 Experimental setup devices. (a) Caterpillar mobile robot (BLIZZARD SR, Kyosyo Corp., 35cm ×30cm ×8 cm) attached red marker (0.18m ×0.18m). (b) Setup of the experiment. Camera (640 pixels ×480 pixels, 30 fps) was attached on the ceiling and two markers (the robot and target) were found by red color image analysis

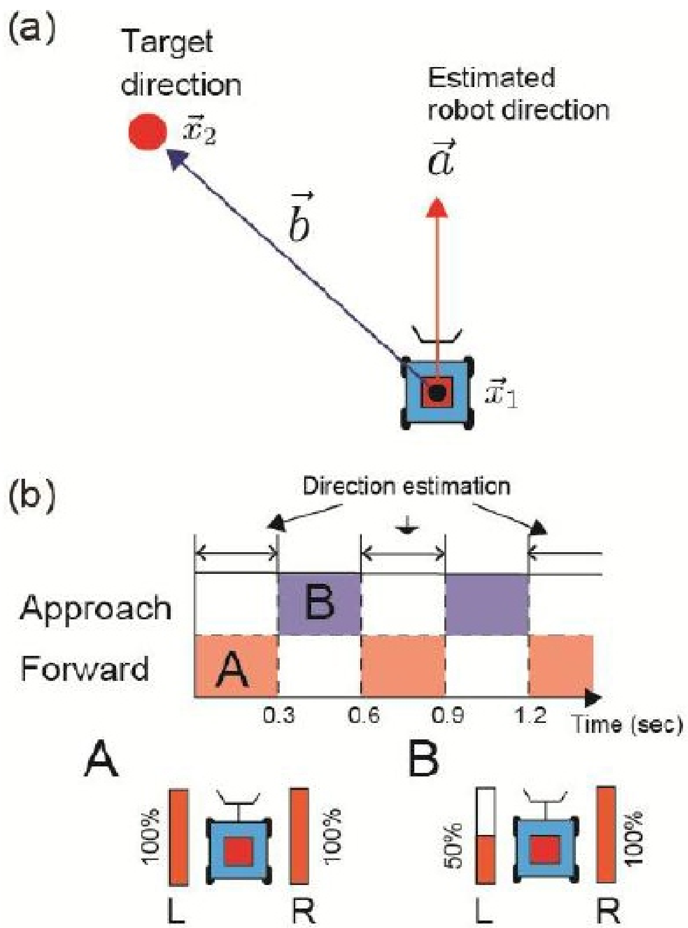

Fig.3 (a) Definition of the vector $\vec{a}$ and $\vec{b}$.(b) Proposed control strategy two phase method.

of the robot denoted by A in Fig.3b. Method (a) was previously proposed general direction estimation algorithm and the caterpillar rotations only were used to estimate the direction in this study. On the other hand, Method (b) was a proposed strategy, and there is two control phases in the strategy - (A) Forward movement phase to estimate which is the head direction of the robot, and (B) Approach phase to control the robot to the target position. In the Forward phase, the R and L channel power balances of the caterpillar robot were set same values eg.100% while 300msperiod, and the red marker position movement was measured and set as $\vec{a}$ in the 300 ms phase. Next approach phase use f_R and f_L as R and L channel powers of the robot defined below in the period of 300 ms,

$$Cross_z = \vec{a} \times \vec{b} \qquad (1)$$

$$f_R = \alpha Cross_z + \beta_R \qquad (2)$$

$$f_L = \alpha Cross_z + \beta_L \qquad (3)$$

where α is constant, β_R and β_L are power bias parameters depended on the machine. The parameters were set to move the robot forward direction if the cross product value $Cross_z$ is zero. In the Method (b) control, the (1) to (3) are used.

IV. EXPERIMENT

Experiment 1 performs basic forward movement test when the right caterpillar power changed 40% to 100% and the left power was fixed 100% (power supply was 12 V DC, the power was changed by 1 kHz PWM and the ON time ratio). Experimental time was 500 ms. From this experiment, the power bias parameters β_R and β_L were determined. The ground condition of the room was flat (polished concrete), but slippy surface for the plastic caterpillar. Experiment 2 performs movement control to the target position on the slippy surface of the polished concrete when Method (a) and (b) control strategy. The area of the experiment was 4 m ×3 m field, and the target position was set (-0.4, 2.3) m from the start position.

Experiment 3 confirms the effectiveness of the outer product. The robot is moved by the control method using the outer product and angle algorithm. Compare the relationship between the distance to the target, the angle, and the value of the outer product.

V. RESULT

Figure 4 represents the trajectory plotting result of experiment 1. The robot was started from (0,0) position. Since 100% plot is tilting to the left side (x,y)=(-0.13,0.45), the movement power of the right motor is large comparing with the left. Even if the power input to the motors were completely same, the real robot movement would be affected by another factor such as caterpillar surface friction, gear friction loss and so on. From this result, the robot was moved to almost straight ahead when the power of R:L = 70%:100%. As a result, we set β_R = 35% and β_L = 50% respectively in later experiment. Figure 5 represents the trajectory plotting result of experiment 2. Red and green circle were start and target position respectively.

Blue colored plot was the result of Method (a) : oddmetry. The trajectory largely deviated to the left side, and the front direction of the robot was different from the target direction (black arrow). Red colored plot was the result of our proposed Method (b). 300 ms periodical "forward" and "approach" switching control could realize the movement control to the target direction even though in the slippy surface of the polished concrete, and the estimated direction a was estimating correctly in all the situation. The mechanism of the Method (b) was summarized in Fig. 6 especially in the slipper situation. If the left caterpillar was slipped in a situation (Fig. 6A), even though the power balance was 50:50, the robot position was moved left top side and the direction also changed at the same time. In the situation B of Fig. 6, the robot performs "Forward" phase (Fig. 3), and the vector a would be obtained. In a small area of the slippy environment, the direction of the a would be a kind of pseudo "straight" direction of the robot. Next in the approach phase, the robot would calculate the wheel power on the condition that the vector a is regarded as "straight" direction in the small slippy area. This periodical control process was assumed in the proposed algorithm, and it could realize the performance of rough terrain movement.

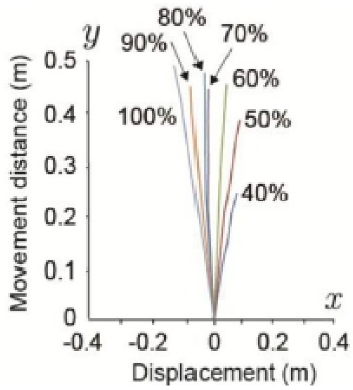

Fig. 4 Result of experiment 1 : basic forward movement test dependency of the right caterpillar power

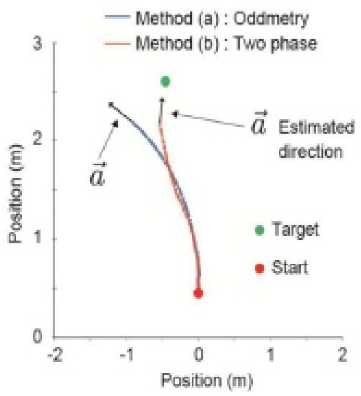

Fig. 5 Result of experiment 2 :ifference of the trajectory of Method (a) and Method (b) control strategy.

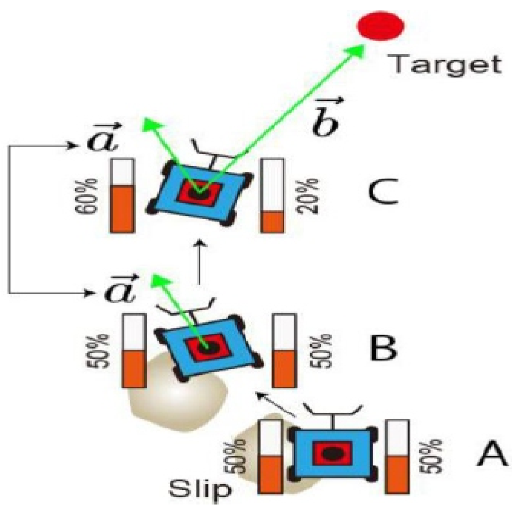

Fig. 6Mechanism of the proposed control Method (b).

Figure 7 represents the trajectory plotting result of experiment 3.Thered and blue lines represent the relationship between the angle and the outer product when approaching the target. As the robot approaches the target, it can be seen that the value of angle gradually increases. On the other hand, it can be seen that the value of the outer product gradually decreases. When the target is far away, the angle value is small, so it is almost straight. However, you need to make a sharp turn because the angle increases rapidly when you get close to the target. However, the robot cannot suddenly turn and cannot reach the target. On the other hand, the outer product value is equal to the area of the parallelogram created by the two vectors, so the farther the distance from the target, the larger the outer product value and the coarse movement. As you get closer, the value of the outer product becomes smaller and moves finely. So you can achieve your goals naturally.

VI. CONCLUSION

In this paper, a mobile robot control strategy of rough terrain capable of position and direction estimation by a single marker was proposed, and the effect was performed. To realize wheel / caterpillar mobile robot movement on the rough terrain such as house farm, it is necessary to solve the precise position estimation and the direction estimation are important before the development of the control theory. This study developed a method to estimate the mobile robot direction using a single marker placed at the top of the robot by changing the front movement and the target direction movement periodically. Experimental result shows that even if there is slip while the forward phase, obtained vector $\vec{a}$ pseudo "straight" direction of the robot, and cross product between $\vec{a}$ and $\vec{b}$ ınnel power control. Our propo-sed method would be effective in the difficult situation to find or analyze the marker position of the robot surfaces by the reason of camera position and the environment, and it could realize wheels / caterpillar type mobile robot movement on the muddy situation.

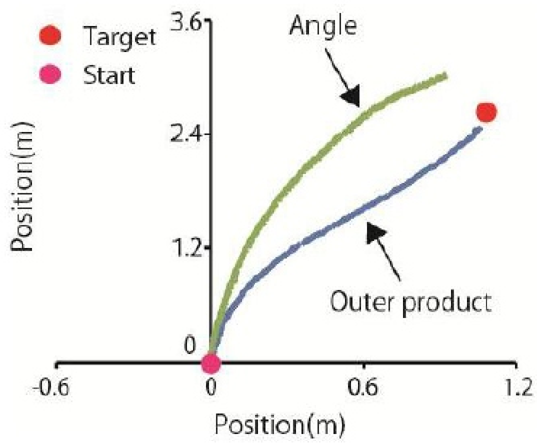

Fig. 7 Result of experiment 3 : Comparison between outer product method and angle method

REFERENCE

[1] S. Chen, B. Mulgrew, and P. M. Grant, "A clustering technique for digital communications channel equalization using radial basis function networks," IEEE Trans. on Neural Networks, vol. 4, pp. 570-578, July 1993.

[2] Daisuke Endo, KeijiNagatani, Kazuya Yoshida, "An advantage of crawler mechanism is a stable navigation on uneven terrain. So many of rescue and field robots adopt such a mechanism. However, the mechanism has a problem of slippage with the ground", Journal of the Robotics Society of Japan, Vol. 33(6), pp. 433-440, 2015. (in Japanese)

[3] Hideki Toda , Hiroaki Takano, Hiroaki Takano, "Effect of Discrete Yaw Direction Setting for 4 Roter Helicopter Control: Computer Simulation and AR. Drone Model Implementation ", International Journal of Innovative Research in Advanced Engineering, Vol. 3, Issue 7, Paper ID JYAE10086, doi:10.17632/cj8f3v6csr.1, July 2016

[4] J. U. Duncombe, "Infrared navigation—Part I: An assessment of feasibility," IEEE Trans. Electron Devices, vol. ED-11, pp. 34-39, Jan. 1959.

[5] C. Y. Lin, M. Wu, J. A. Bloom, I. J. Cox, and M. Miller, "Rotation, scale, and translation resilient public water marking for images," IEEE Trans. Image Process., vol. 10, no. 5, pp. 767-782, May 2001.

ISSN Print : 2320-2084, Online : 2321-2950

Proposal of Estimation Method using the Absolute Angle of A Geomagnetic Sensor for Instability of Distance Information of Lidar Caused by Moving and Vibrating Objects

[1]SHINYA HAMA, [2]HIDEKI TODA
[1,2]Dept. of Electric and Electronic Engineering, University of Toyama Gofuku Campus, 3190 Gofuku, Toyama, 930-8555, Japan E-mail: m1871027@ems.u-toyama.ac.jp

ABSTRACT

In this paper, we propose a method to improve the strength by using a geomagnetic sensor to perform self-angle estimation using moving objects such as wall and a vibrating object such as human or trees trembling by wind more stably. LIDAR sensor used time of flight information of laser to measure the distance from the target, the micro or Nano second-order time difference would be disturbed by a few physical factors - sensor movement/vibration, target shape complexity, and target movement/vibration. Therefore, the angle estimation is easily disturbed for the features of moving objects and vibrating objects. This is a problem that inevitably occurs in the measurement principle of LIDAR. For this reason, it is necessary to strengthen the angle estimation using not only LIDAR but also a sensor that gives auxiliary information at the time of angle estimation. We focused on geomagnetic sensors that can obtain absolute angles among sensors that can get angle information.We propose a robust angle estimation method using the angle information of the geomagnetic sensor as auxiliary information for localization by LIDAR. The experimental result of experiment 1 shows that even if the object was straight shape board, there was a directional dependence of object movement for angle estimation based on the ICP algorithm. There was a significant effect to (B) back direction movement, and it was related to reducing the measurement points of the LIDAR. However, the proposed method can reduce the self-angle estimation error in all directions by more than 95.62%. In the case of vibration object made with green ribbons, the proposed method was able to follow the angle change and the estimated angle also changed, enabling stable angle estimation. And, the proposed method can reduce the self-angle estimation error in all directions by more than 99.75%. Our experimental result shows that there is a weak direction to move the LIDAR sensor itself, and it is a complicated process to estimate the rotation angle by ICP when the object is vibrating or moving. However, stable estimation was made possible by using a geomagnetic sensor to assist in angle estimation.

Keywords - Geomagnetic Sensor,Icpalgorithm, Lidar,Moving and Vibrating Object.

I. INTRODUCTION

The government and companies cooperate, and the technology development of automatic driving is progressing actively for the aim of practical application by 2020 [1]. To realize autonomous car control without human, the correct, current position estimation (localization) is an essential factor, and it would be measured by LIDAR device generally. LIDAR (Light Detection and Ranging) is used as an essential device for recognizing the surrounding environment like human eyes and ears. LIDAR uses time of flight (TOF) information of laser to measure the distance from the target, the micro or Nano second

-order time difference. It would be disturbed by some few physical factors - sensor movement/vibration, target shape complexity, and target movement/vibration(Fig. 1).

In the previous study, we confirmed the instability in angle estimation using ICP (Iterative Closest Point) algorithm [1]-[5] with the object that disturbs the LIDAR data as the measurement object. Even the slight movement of the object itself, as shown in Fig. 1, has similarly collapsed. Besides, the estimation collapsed even with a change of only a few centimeters in the shape of the object, such as a tree branch or leaf shaking. There are two significant reasons for this because of the characteristics of the estimation algorithm. First, as shown in Fig. 2, for example, a broad-angle change is assumed. At that time, due to the characteristics of the ICP algorithm that determines the nearest neighbor as a corresponding point, there is a high possibility of selecting an incorrect corresponding point. Therefore, once the estimated value deviates from the actual value, it is difficult to return to the correct estimated value. It is because the error is included in the next estimation. The second is when measuring unknown environmental point clouds, as shown in Fig. 2(b). Localization by LIDAR is a matching between the measurement point cloud and the corresponding past measurement point cloud. However, since there is no past point cloud corresponding to the unknown point cloud, it causes a false estimation. When moving objects and vibrating objects are measured using LIDAR, there is a very high probability that they have never been measured before. Therefore, the angle estimation is easily disturbed for the features of moving objects and vibrating objects. This is a problem that inevitably occurs in the measurement principle of LIDAR. For this reason, it is necessary to strengthen the angle estimation using not only LIDAR but also a sensor that gives auxiliary information at the time of angle estimation. In this paper, we focused on geomagnetic sensors that can obtain absolute angles among sensors that can get angle information. We propose a robust angle estimation method using the angle information of the geomagnetic sensor as auxiliary information for localization by LIDAR.

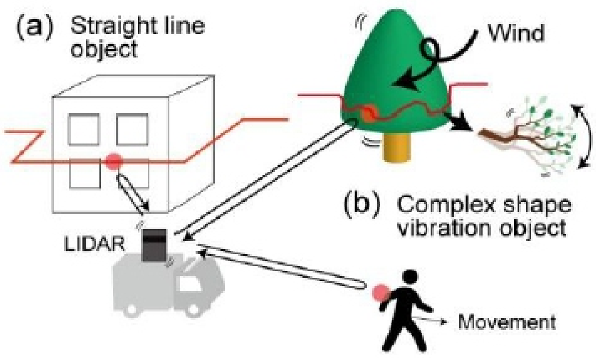

Fig.1.Some factors of noise appearing on the LIDAR sensor. (a) Astraight-line shaped object such as a wall or building. (b) Complex shapeand movement/vibration object.

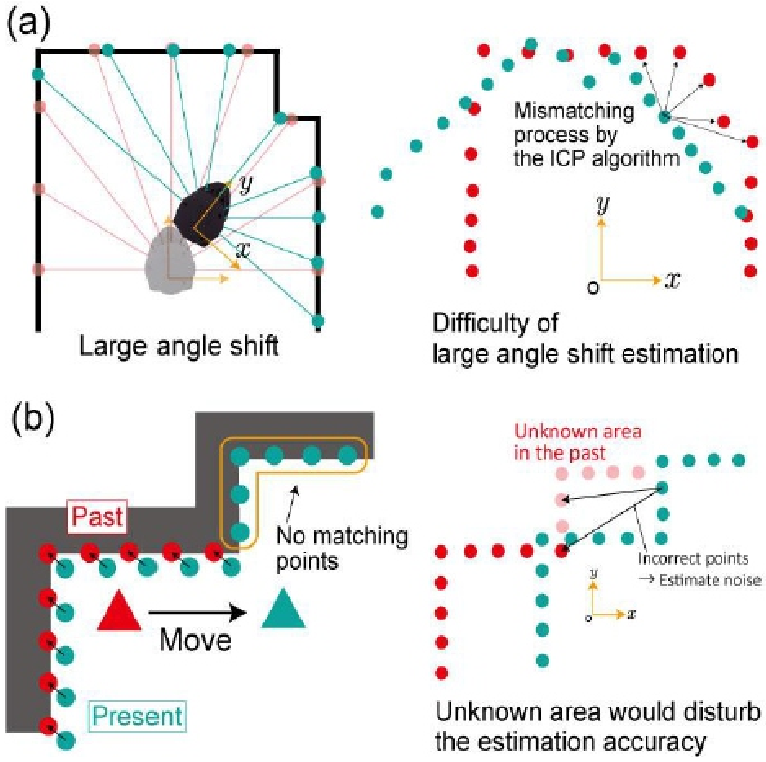

Fig.2.The difficulty of rotation angle estimation process by using the ICPalgorithm. (a) The angle changes significantly, and the corresponding pointis wrong. (b) The points in the unknown area do not have correspondingpoints and become noise during estimation.

II. METHOD

In this paper, we propose a method to improve the strength by using auxiliary information using a geomagnetic sensor effectively in order to perform self-angle estimation using moving objects and vibrating objects more stably. Many sensors can assist in angle estimation. Among them, the reason we focused on geomagnetic sensors is that we can obtain absolute angles. For example, the gyro sensor can calculate the current aircraft angle by integrating the acquired angular velocity data, but a calculation error always occurs. The angle detection by the camera does not change from the point cloud matching by LIDAR to the estimation by image matching. Therefore, the estimation error occurs in the same way, and it does not solve the fundamental problem. Thus, in the self-angle estimation using the relative angle, the origin gradually drifts due to the estimation error. However, the geomagnetic sensor can obtain the absolute angle from the origin to the magnetic north by detecting the geomagnetism. Since the geomagnetic sensor detects a weak magnetic field in nanometers, the sensor reacts sensitively even if a slightly magnetized object exists in the surroundings. If the angle information of a sensitive sensor is used as a trap, there is a information of a sensitive sensor is used as a trap, there is a problem in applying it to angle estimation that can lead to system collapse even with an angle error of 1 degree. Therefore, we focused on the information about which direction the sensor is facing rather than the information of angle, and used it as auxiliary information for angle estimation by LIDAR.

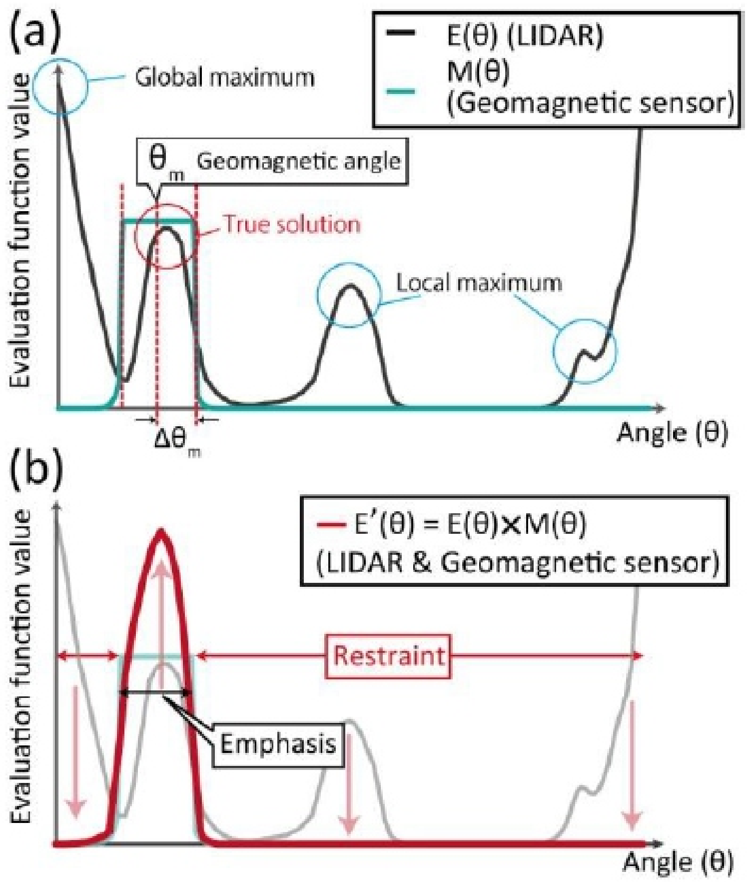

Fig.3. Evaluation function used for angle estimation in the proposed method using geomagnetic sensors. (a) E(θ) is an evaluation function by LIDAR, and M (θ) is an evaluation function by a geomagnetic sensor. (b) E′(θ) is an evaluation function using LIDAR and a geomagnetic sensor.

$$\mathrm{E}(\theta) = \sum_{i=1}^{m} exp(-\alpha\|\vec{b_i} - R(\theta)\vec{a_i}\|^2) \quad (1)$$

$$\mathrm{R}(\theta) = \begin{pmatrix} cos\theta & -sin\theta \\ sin\theta & cos\theta \end{pmatrix} \quad (2)$$

$$\mathrm{M}(\theta) = \begin{cases} \beta \ (|\theta_m - \theta| \le \Delta\theta_m) \\ 0(|\theta_m - \theta| > \Delta\theta_m) \end{cases} \quad (3)$$

Figure 3 shows the evaluation function for angle estimation using LIDAR and geomagnetic sensor described in this paper. The black line is the evaluation function based on the point cloud data of LIDAR and is defined as in (1) $\vec{a_i}$ is the previous measured point set represented as (x,y) axis, a$\vec{b_i}$l . is the present measured point data set.Ris a rotation matrix and uses an exponential function that takes the negative of the normal ICP matching evaluation function and uses the Napier's constant e as the base. As a result, the angle θ where the difference between $\vec{a_i}$and $\vec{b_i}$ becomes small is noticeable, and the angle estimation is stabilized by suppressing the function values of other parts. The coefficient α was set to 0.02. The angle θ is estimated by maximizing the evaluation function E using the Euler method. The problem here is convergence to the local solution during estimation. In the evaluation function E

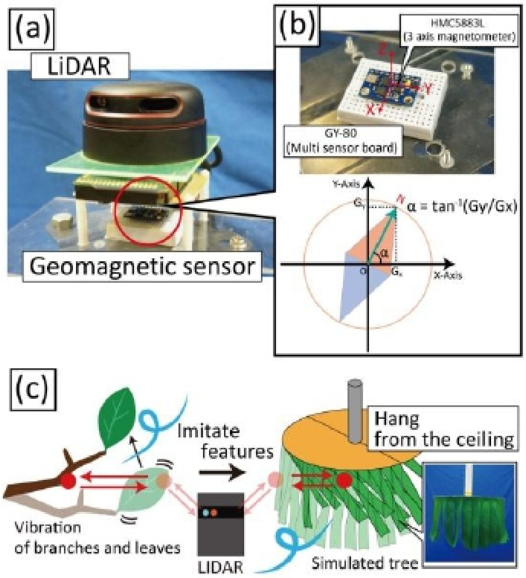

Fig.4. Experimental setup devices. (a) LIDAR sensor (RPLIDAR A2, SLAMTEC Corp, Measurement distance 0.15-6 m, range 360 degrees, measurement accuracy 1 %, 2000 samples/s). (b) Geomagnetic sensor (HMC5883L - 3-Axis magnetoresistive Sensors, Field Range ± 8 Gauss, Noise Floor 2 milli-gauss, Compass Heading Accuracy 1-2 Degree). (c) The ribbon is shaken by the wind of about 2 m/s. As a result, the structure can reproduce the wind fluctuations of the branches and leaves of the plant.

using the LIDAR point cloud data of the black line, there are many local solutions where the function value is the maximum when viewed locally. There is also a possibility that the optimal solution that is the global maximum is not correct. It is because an incorrect corresponding point is selected, but it inevitably occurs in the ICP matching algorithm, as shown in Fig.2 (a). The green line is an evaluation function using the angle θm and is defined as in (3). The angle $\Delta\theta_m$ is emphasized around the angle θ_m, and the others are suppressed. The coefficient β was set to 10. Also, $\Delta\theta_m$ was set to 5 degrees considering the error of the geomagnetic sensor. As a result, the maximum value of the evaluation function existing in a specific direction can be emphasized by connecting with the evaluation function E by LIDAR, and the local solution living in the evaluation function can be eliminated by suppressing the others.

III. EXPERIMENT

Angle estimation using a geomagnetic sensor is performed in the presence of moving objects and irregular objects. The effectiveness of the proposed method in the environment shown in Fig.1 is proved. Figure 4 (a),(b) show the LIDAR and geomagnetic sensor used in the experiment. The natural environment cannot quantitatively evaluate the characteristics of the environment, and the reproducibility of the experiment is low. Therefore it is necessary to conduct experiments in an environment that simulates the natural environment to confirm the cause of the conventional problem and the reproducibility of the proposed method. Therefore, we created a simulated tree, as shown in Fig.4 (c) that simulated the characteristics of the vibrating object.

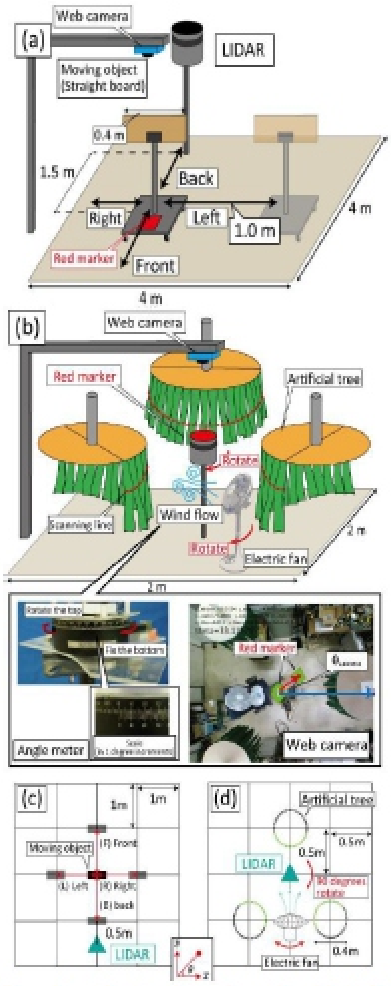

Fig.5. Experimental setup of experiment 1 and 2. (a) Straight shape boardobject movement strategy in experiment 1. (b) Artificial tree vibrating objectsetup of experiment 2. (c) Two-dimensional plan view of Experiment 1. (d)Two-dimensional plan view of Experiment 2

The simulated branches and leaves are made by adhering a polyester ribbon with a length of 250 mm, a width of 40 mm, and about 2 g to the half of the circumference of a disk with a whole range of 400 mm.By hanging from the ceiling, it can move even with a small amount of wind and can have a random swinging motion due to the lightness of the ribbon and the swing function of the fan.

In Experiment 1, self-angle estimation is performed in an environment with moving objects. The effectiveness of the proposed method is shown by comparing the proposed estimation method with the conventional method.

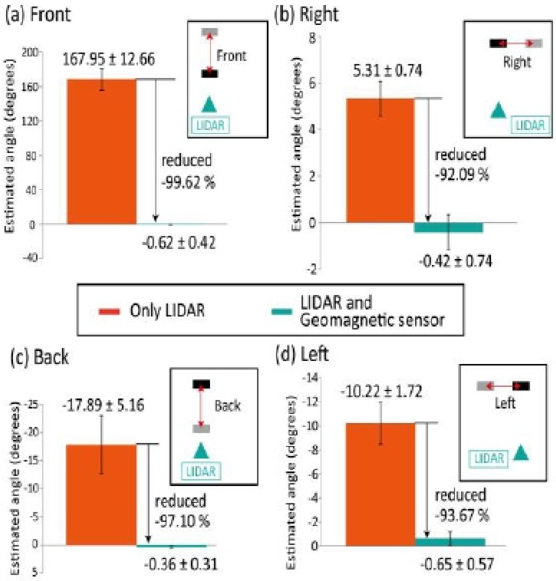

Fig.6. Result of experiment 1. 0.4 m_0.2 m straight shape board movement case (N=5). (a) Forward, (b) Right, (c) Backward and (d) Left direction.

Fig.5 (a),(c) shows the straight board movement experimental setup (experiment 1).The 0.4 m×0.2 m straight board was positioned on the 1.5 m front of the LIDAR sensor, and the board was moved 1 m distance from the original position with 0.25 m/s to (L) left, (R) right, (B) back and (F) front direction. After that, it was returned to the original position. The area of the measurement was limited at a black line square 3 m×3 m area to reject another objects except for the board. A web camera (640 pixels×480 pixels, 30 fps) is installed on the ceiling, and a red marker (0.18 m×0.18 m) is attached to the moving object. Clustering was performed for red in the image data, and the movement trajectory of the moving object was determined. Next experiment 2, the experimental setup was shown in Fig.4 (b),(d).In Experiment 2, self-angle estimation is performed in an environment with vibrating objects. After rotating 90 degrees, it turned to the initial angle and returned to the initial state. Thus, it is shown that stable angle estimation can be performed even if the angle changes by using the proposed method. An environment surrounding LIDAR was created using three simulated trees that quantitatively mimic the characteristics of a vibrating object. LIDAR measurement is limited to the range of 1 m×1 m, and it reproduces the estimated environment in forests where there are many irregular objects. From the electric fan, wind at a wind speed of 2 m/s is applied to the simulated tree to reproduce the wind fluctuation of the branches and leaves of the plant. The standard deviation (S.D.) of the ribbon vibration was measured as 4.6 cm in the case of 2 m/s wind flow. In order to know the actual value of the estimated angle, a web camera is installed on the ceiling directly above LIDAR. Two red markers (6.5 cm×6.5 cm) were attached to the LIDAR unit, and the actual angle was determined from the coordinate data on the web camera. Besides, the accurate rotation was performed using an angle meter.

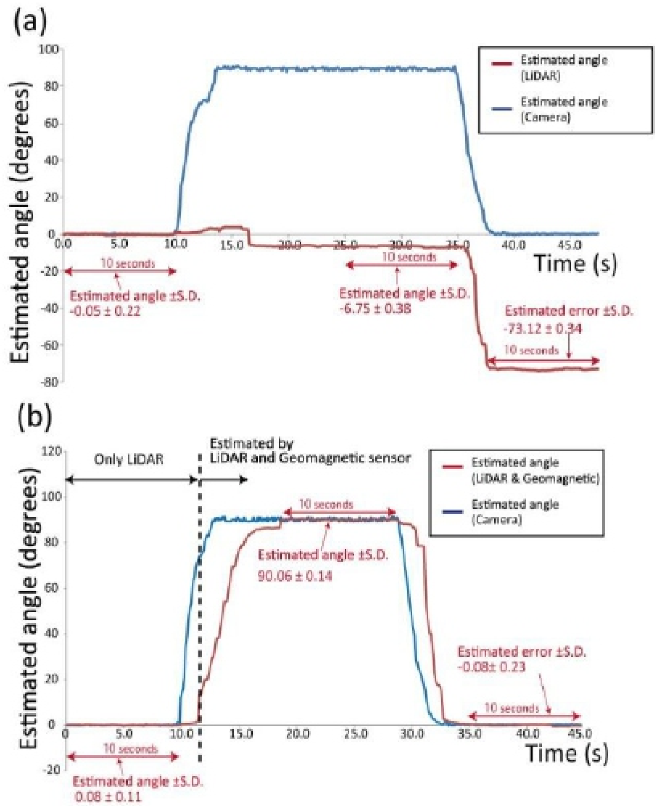

Fig.7. Result of experiment 2. The artificial tree vibrating object case. (a)The result of the conventional method using the only LIDAR. (b) The resultof the proposed method combining the geomagnetic sensor and LIDAR.

IV. RESULT

Fig.6 shows the rotation angle θ estimation result of the straight board object movement. Fig. 6 (a) shows the estimated self-angle after moving the straight board object in the forward direction and returning it to the original position. Similarly, (b) is the right direction, (c) is the backward direction, and (d) is the left direction self-angle estimate. This is the final self-angle estimate (average±standard deviation, 5 trials) in 5 seconds after returning to the original position. In the case of (b) right direction movement, the estimated θ was shifted about 5.31±0.74 degrees by moving 1m of the straight board object. The proposed method was -0.42±0.74 degree, and the self-angle estimation error could be reduced by 92.09%. In the case of (d) left direction movement, the estimated θ was shifted about -10.22±1.72 degrees by moving 1m of the straight board object. The proposed method was -0.65±0.57 degree, and the self-angle estimation error could be reduced by 93.67%. Regarding (b) and (d), the average number of distance measurement points of the straight board was about 7 points during the experiment. Next, in the case of (c) backward direction movement, the estimated θ was shifted about -17.89±5.16 degrees by moving 1m of the straight board object. The proposed method was -0.36±0.31 degree, and the self-angle estimation error could be reduced by 98.0%. Last, in the case of (a) forward direction movement, there is large unstable θ estimation error about -167.95±12.66 degrees, and the estimation could not recover by moving 1m of the straight board object.

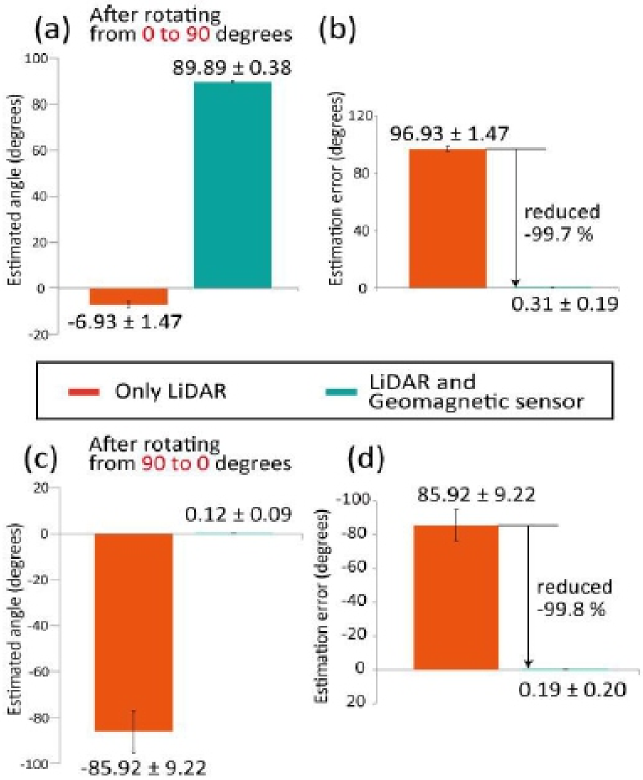

Fig.8. Result of experiment 2. 0.4 m_0.2 m artificial tree vibrating object case (N=5). (a) Self-position estimation result when rotated 90 degrees. (b)Self-position estimation error in (a). (c) Self-position estimation result when rotating to the original position. (d) Self-position estimation error in ©.

But, the proposed method was -0.62±0.42 degrees, and the self-angle estimation error could be reduced by 99.62%. In the (a) forward movement case, the average number of measurement points was about 3.5 after the 1 m movement. Experiment 1 result clearly shows that there was movement direction dependency even if the target was straight board shape. Even when the number of LIDAR measurement points was reduced, and the estimation error increased (a), the estimation method could eliminate the estimation error. Fig.7 and Fig.8 shows the result of self-angle estimation using a simulated tree. Fig.7(a) shows the result of the conventional method using the only LIDAR. Red is the estimated angle, and blue is the trajectory of the angle change obtained from the camera. Although it was rotated 90 degrees from the initial angle, the estimated angle was -6.75±0.38 degrees. After that, the angle was returned from 90 degrees to 0 degrees, but the estimated angle was -73.12±0.34 degrees. Fig.7 (b) shows the result of the proposed method combining the geomagnetic sensor and LIDAR. Similarly, when rotated 90 degrees, the estimated angle was 90.06±0.14 degrees. After that, when the angle was returned from 90 degrees to 0 degrees, the estimated angle was -0.08±0.23 degrees. Fig.8 shows the results of five experiments using each method. This is the final self-angle estimate (average±standard deviation, 5 trials) in 10 seconds after rotating to the 90 degrees and initial angle. The conventional method had a significant influence on the estimated angle θ, despite the minute vibration of the ribbon about 4.6 cm. In contrast, the proposed method used the auxiliary angle information from the geomagnetic sensor to prevent erroneous estimation in the estimation calculation. As a result, the self-angle estimation was stable without any disruption.

V. CONCLUSION

In this paper, we propose a method to improve the strength by using auxiliary information using a geomagnetic sensor effectively in order to perform self-angle estimation using moving objects and vibrating objects more stably. The experimental result of experiment 1 shows that even if the object was straight shape board, there was directional dependency of object movement for angle estimation based by ICP algorithm. There was large effect to (B) back direction movement, and it was related to reducing the measurement points of the LIDAR. However, the proposed method can reduce the self-angle estimation error in all directions by more than 95.62%.In the case of vibration object made with green ribbons, the proposed method was able to follow the angle change and the estimated angle also changed, enabling stable angle estimation. And, the proposed method can reduce the self-angle estimation error in all directions by more than 99.75%.

REFERENCE

[1] S. Rusinkiewicz and M. Levoy, ”Efficient Variants of the ICP Algorithm”,3-D Digital Imaging and Modeling, pp.145-152, 2001.

[2] J.S. Gutmann, T. Weigel, and B. Nebel, ”Fast, Accurate, and RobustSelf-Localization in Polygonal Environments”, Proc. of IROS’99,pp.1412-1419, 1999.

[3] G. Grisetti, C. Stachniss, and W. Burgard, ”Improved Techniques forGrid Mapping with Rao-Blackwellized Particle Filters”, IEEE Trans.on Robotics, vol. 23, no. 1, pp. 34-46, 2007.

[4] MILT, ”Main goverment policies concerning automatic driving”, URL:https://www.mlit.go.jp/ jidosha/ jidousha tk7 000018.html, (accessedon 2018 March). (in Japanese)

[5] P.J. Besl, Neil D. McKay, ”Method for registration of 3-D shapes”,IEEE Transactions on Pattern Analysis and Machine Intelligence, Vol.14, Issue 2, pp. 239-256, Feb. 1992.

Proposing an Ankle Joint Lifting Mechanism of Ankle Joint Pushing Machine Concerning About Sense of Firmness

[1] Takahisaino, [2] Hideki Toda
[1,2] Dept. of Electric and Electronic Engineering, Faculty of Engineering, University of Toyama
E-mail: [2]toda@eng.u-toyama.ac.jp

ABSTRACT

In this paper, an ankle joint lifting mechanism of ankle joint pushing machine concerning about sense of firmness was proposed, and the effect of the mechanism was examined in the system. The stretching of the ankle joint is an important medical treatment that physical therapist (PT's) utilize to help their patients recover their ability of walk and to prevent contracture. Since the ankle treatment requires a large amount of force (nearly equal to the subject's weight), precise angle and power controls, manual treatment by PTs has not been replaced by mechanical treatment systems. Before the ankle joint stretching treatment, the knee joint of the subject is necessary to extend straightly for maximizing the therapeutic effect of the ankle joint. However, there is few proposal to lift up the lower leg horizontally without pain. To realize the lifting up mechanism of the lower leg without pain, the developed system uses two linear actuators to ease the pain during the lift-up process. By using two actuators to lift the lower limb to horizontal position, the positional deviation between the ankle joint and rotation center of the device was measured $\Delta \mathbf{y} = 87$ mm *On the contrary, in the condition of using a single actuator to lift the lower limb, the positional deviation was measured* $\Delta \mathbf{y} =295$ mm. *There is 295-87= 208 mm distance displacement between the ankle joint and the device rotation center if a single actuator would be used to lift the lower limb process. The proposed two actuators lower limb lifting mechanism will effectively work to develop ankle joint stretching system.*

Keywords - Ankle Joint Pushing Unit Mechanism, Ankle Joint Stretching System With Two Linear Actuators , Change the Length System, Leg Lifting Mechanism

I. INTRODUCTION

Ankle is an indispensable body part to carry out daily activities such as walking, running, sitting and so on. It is ruggedness enough to withstand a heavy load that is received in daily life. If the ankle joint could not work for a long time due to sickness or injury, it will suffer an ankle joint contracting state [1]-[2]-[3]. As a general ankle contracture prevention treatment, physical therapists(PT) perform the ankle joint stretching by manual therapy (Fig. 1(a)). Manual therapy has advantages to push the ankle joint by a large force safely, easier to deal with the reactions of the patient, but it is necessary to apply the force equivalent to the body weight in order to stretch the ankle joint. In addition, it requires about 20 to 40 minutes of exercise at one time, it is hard work for PTs [1]-[3]. On the other hand, ankle joint pushing machines has been tried to develop for a long time, however, the difficulty of the precise power and angle control without causing the patient any pain has been stopped the mechanization [4]-[5]-[7]-[8]-[9].

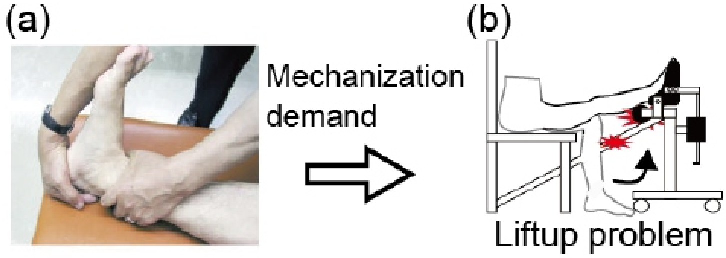

Fig.1 One of important medical treatment that PT's of stretching of the ankle joint utilize to help their patients recover their ability to walk and to prevent contracture, and the demand of the mechanization.

As our previous study [6], we could realize a stable ankle joint pushing mechanism by using a brace structure that is able to manage with the reaction force generated during foot sole pushing process to prevent deviation of the device rotation axis. However, from the viewing of user side, the user must lift up their leg to the ankle joint pushing device as shown in Fig. 1(b) before the ankle joint pushing treatment. It has been a hard work for the subject for a long time. This paper focused on the leg lifting mechanism before the ankle joint pushing treatment, and the mechanism is realized by the two linear actuator equipped under the subject sitting chair (Fig.2).The proposed mechanism will improve the ease of the ankle joint rehabilitation system.

II. PROPOSED ANKLE JOINT STRETCHING MECHANISM INCLUDING LEG LIFTING MECHANISM

Figure3(a) shows that proposed ankle joint pushing treatment system including leg lifting mechanism. The device was made of the subject sitting chair, ankle joint pushing mechanism and the leg lifting mechanism by using two linear actuators. The leg lifting mechanism was connected to the chair. The actuator 1 (ECO-WORTHY LINEAR ACTUATOR, length 400 mm type) was connected to the center of the chair leg and the actuator 2, and it could lifts the actuator 2 (same with actuator 1, length 250 mm type) from 0 to 90 degrees. In addition, the actuator 2 can change the length between 390 mm to 640 mm from the terminal of the chair (position was just below the knee). Main reason of the using two actuator system is to consider a similar effect of the Senuki that have been known by PT for a long time (Fig. 3b). This Senuki effect has been affected to the bedridden subject as the skin tension or thepulling tension, and it leads uncomfortable tension and the pain that tears weak the skin when the backrest rising of the electrical bed.

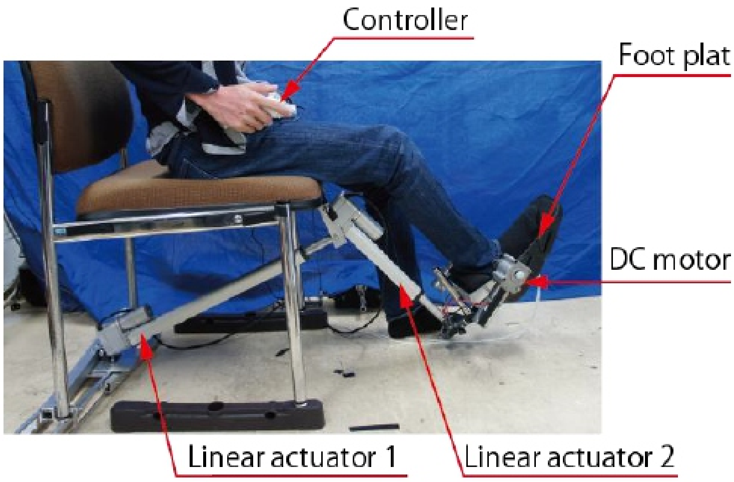

Fig.2 Developed ankle joint stretching mechanism including subject leg lifting mechanism.

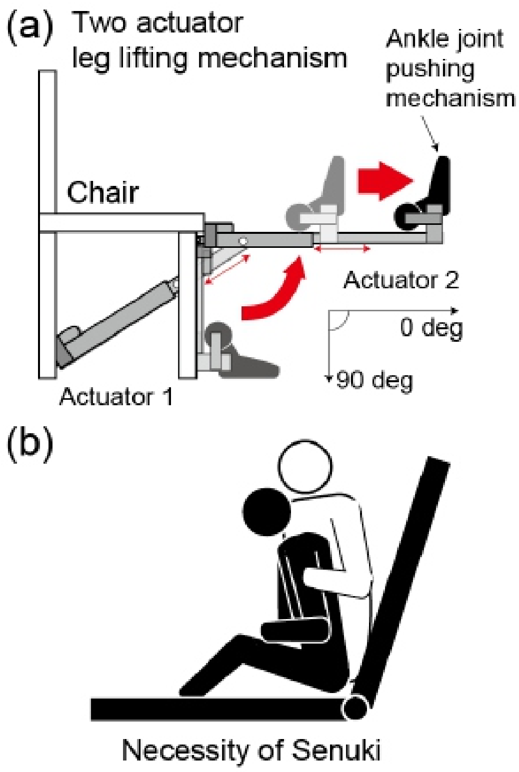

Fig.3 (a) Basic concept of the leg lifting mechanism of the ankle joint stretching system with two linear actuators.(b) Necessity of Senuki.

The Senuki process was, when the raising the electric bed, the caregiver holds the patient, removes the patient from the bed, removes the tension feeling, and then returns the patient to the bed again. It have to be done every time when the raising the electric bed. If the leg lifting process would be realized by one actuator, uncomfortable feelings will occur at the subject leg while the leg lifting process. It is generally caused by the difference of the position between the knee and the rotation center of the leg lifting actuator. About the ankle joint pushing, Fig. 4 shows the ankle joint pushing mechanism [6]. It is constructed from three parts: (a) Foot plate, (b) two DC motors and (c) Foot rest. The proposed ankle joint pushing mechanism is here: (1) By placing the Achilles tendon on the (c) foot rest, it is easy to align the ankle joint and the pushing axis of rotation by the Two DC motors are attached to the side of the frame, and rotate the Footplate dorsiflexion or plantar direction.

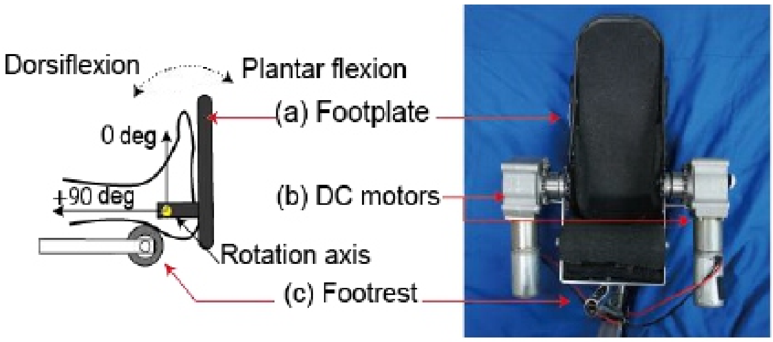

Fig.4 Ankle joint pushing unit mechanism.

(b) DC motors. So, any pain is occurred in the ankle and the heel. (2) By using the patient weight when using the device, it is not necessary to fix the patient's leg and the device with the belt, so pains on the patient's foot is not applied. By combining above the leg lifting and the ankle joint pushing mechanisms, a less discomfort ankle joint pushing machine would be able to developed.

III. EXPERIMENT

A. Experiment 1: Lifting up subject's leg by the proposed mechanism

In experiment 1, the difference in the leg lifting process between using one actuator (condition A) and using two actuators (condition B) were confirmed by the developed system. Measurement set up of the experiment is shown in Fig. 5, total five reflection marker points are realtimely measured by a motion capture system (Flex 3, 0.3 MP (640times480, 100 fps), OptiTrack), and one subject (age 21, adult man) is participated in the experiment. The subject was trained the process of the setup and usage of the system. Especially, because the correct ankle joint position is hidden behind the ankle joint pushing mechanism (DC motors), two of reflection markers that are placed every 20 cm are used for estimating the correct ankle joint position (A of Fig. 5). Other marker positions are the knee joint, the hip joint and the device ankle joint rotation center. Experimental procedure (condition A) is here; Firstly, the subject sits the chair and bends his leg 0 degrees position. Next, the leg position is moved from 0 degrees to 90 degrees during 20s by only using the linear actuator 1 in Fig. 5, and the motion captured positional movement of the five markers are analyzed after the experiment. Next experimental procedure (condition B) is that the procedure is same with the condition A, except for the leg position is moved from 0 degrees to 90 degrees during 20s by using two linear actuators 1 and 2 simultaneously. In this case, the speed of the actuator 1 and 2 are 5.7 mm/s respectively.

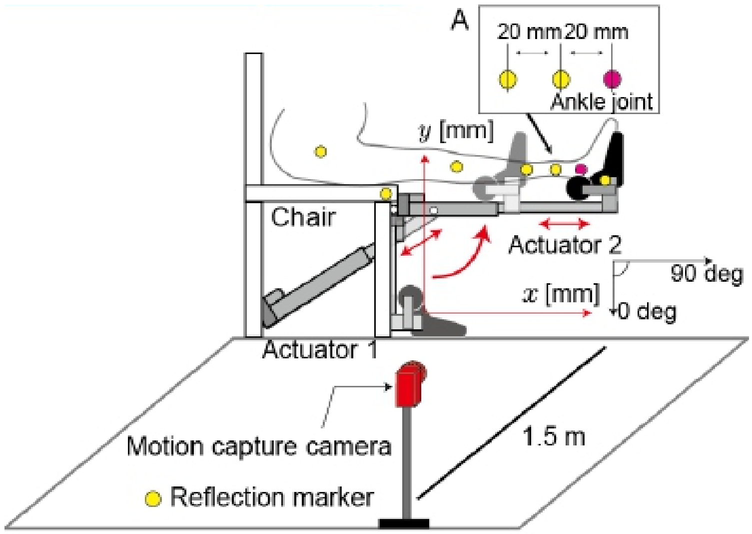

B.3.2Experiment 2: Relationship between the subject lifted leg angle and the ankle joint pushing treatment stability

In the experiment 2, the relationship between the subjects lifted leg angle and the ankle joint pushing treatment stability is confirmed. The setup of the experiment is shown in Fig. 5, and it is same with the experiment 1. Experimental procedure is that the subject sits the chair and bends his leg 0 degrees position firstly. Next, the ankle joint pushing unit is actuated, and the ankle joint is bended about +20degrees for dorsiflexion side (direction and variables are defined at Fig. 4). Third, the ankle joint pushing unit is actuated about +20 degrees for dorsiflexion side when the leg lifting angle is 45 degrees by using the actuator 1 and 2 simultaneously (the actuator moving condition is same with the condition B of Exp.1). Last, the ankle joint pushing unit is actuated about + 20 degrees for dorsiflexion side when the leg lifting angle is 90 degrees.

IV. RESULT

Figure 6 shows experimental result of the effect of the leg lifting mechanism by using one linear actuator (condition A) and two linear actuator (condition B). Horizontal and vertical axis show the motion captured x (mm) and y(mm) axis during 30s leg lifting process. Black solid line shows the hip, ankle, knee joint movement trajectories when the subject lift his leg by himself. In this case, the leg lifting mechanism was not worked. The ankle joint was moving upward taking a circular trajectory, and the knee joint was moving Δy= -86 mm upward (F of Fig.6) during the leg lifting period. It is because that it is necessary to lift the knee slightly before lifting the foot and then extend the foot. Even if the 86 mm upward movement of the knee, the ankle joint trajectory was performed as a perfect circle.

Blue solid lines show the ankle and knee joint movement trajectory when using one linear actuator 1 (condition A). By extending the length of the linear actuator 1, Black solid line shows the leg lifting by subject himself.

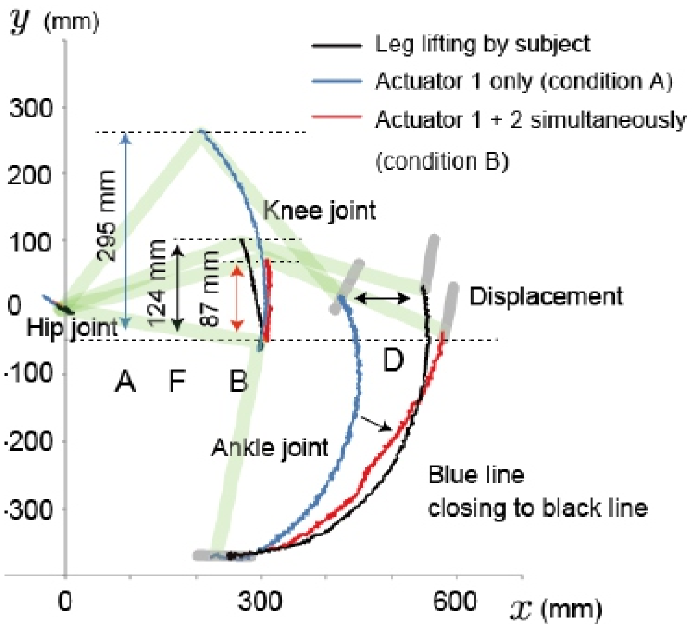

Fig.6 Result of experiment 1.

Blue solid line shows the ankle and knee joint movement trajectory when using one linear actuator 1 (condition A). Red solid line shows the ankle and knee joint movement trajectory when using two linear actuators 1+2 (condition B).the ankle joint pushing bucket was moving upward, however, the movement was not taken a kind of circular trajectory, and the last ankle joint position was shifted D=Δx=- 100 mm comparing with the position of the lifting the leg by himself case. In addition, the knee joint was also moving upward direction (movement distance is Δy= -295 mm, A of Fig.6). The movement of the knee joint was large (Δy=-295 mm) comparing with the leg lifting him case (Δy= -124 mm). At last, the red solid line shows the ankle and knee joint movement trajectory using two linear actuators 1 and 2 simultaneously. Basically the shape of the red trajectory was close to the black trajectory, especially comparing with the blue line. The vertical axis movement distance was Δy=-97 mm, and it is almost same with the case of the subject lifting his leg by himself (Δy = -124 mm). It means that lifting the leg using two actuators simultaneously indicates less stress on the subject than lifting the leg on its own. As basic strategy, by minimizing theΔy, this mechanism would work well and Δy would use as one evaluation indicator to develop the actuator movement control design. Figure 7 shows the result of the ankle joint pushing treatment stability in the case 0, 45 and 90 degrees of the leg lifting mechanism. Horizontal and vertical axis show the motion captured x(mm) and y(mm) axis during 15 s ankle joint stretching process from 0 to 45 degrees by the DC motor ankle joint pushing unit. The case of 0 degrees condition (Fig.3a) was shown as blue points and the ankle position was moved about 120 mm distance by the ankle joint pushing process. This means that by pushing the toe by the DC motor, the ankle joint position was moved upward direction easily since the knee joint could bend.

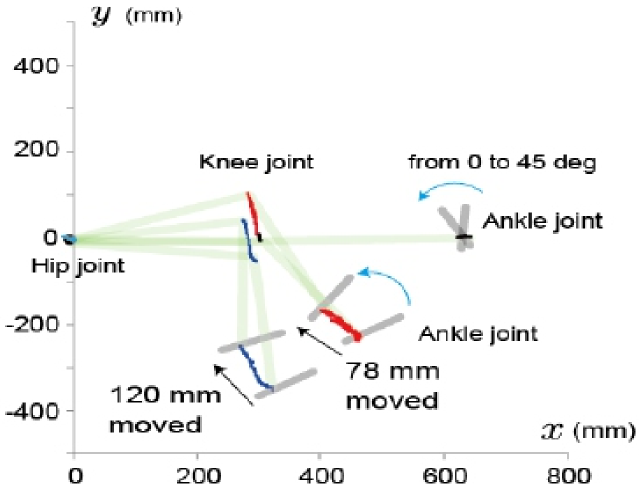

Fig. 7 Result of experiment 2: Meaning of the knee joint bending angle for ankle joint stretching

In this case, the ankle joint was not bended enough, and just the ankle joint and knee joint position was shifted upward. Almost same effect was measured in the case of 45 degrees ankle joint pushing process (red points). The ankle joint was slightly bended in this case, and the ankle joint position was moved 78 mm (less than 0 degrees case). On the other hand, the case of 90 degrees condition was shown as black points and the ankle joint position was not moved during 0 to 45 degrees ankle joint pushing process by the DC motor, and more importantly, the knee joint was also not moved (black points of the knee joint). In this case, the ankle joint was bended enough from 0 to 45 degrees. This means that to realize the precise ankle joint stretching, maintaining to extend the leg straight is very important.

V. CONCLUSION

In this paper, an ankle joint lifting mechanism of ankle joint pushing machine concerning about sense of firmness was proposed, and the effect of the mechanism was examined in the system. To realize the safety and comfortable mechanism of the ankle joint pushing treatment, the developed system have introduced the two linear motors actuated leg lifting system, and the effect of the leg lifting system was confirmed by two experiments. By using two actuators to lift the lower limb to horizontal position, the positional deviation between the ankle joint and rotation center of the device was measured Δy= 87 mm. On the contrary, in the condition of using a single actuator to lift the lower limb, the positional deviation was measured Δy=295 mm. There is 295-87= 208 mm distance displacement between the ankle joint and the device rotation center if a single actuator would be used to lift the lower limb process. In addition, to develop the ankle joint stretching mechanism, the angle of the knee joint is primary factor for effective ankle joint pushing mechanism. The proposed two actuators lower limb lifting mechanism will effectively work to develop ankle joint stretching system.

REFERENCE

[1] Mero. A., Komi. P. V. and Gregor. R. J., "Biomechanics of sprint running," A Review. Sports Medicine. Vol. 13, No. 6, pp. 376-392, 1992

[2] Suzuki Rie, Ohta Yuji, "Causes and preventions of Articular Contracture, " Journal of Human Environmental Engineering, Vol. 9, No.1, pp. 142-143, 2007

[3] Williams PE, "Use of intermittent stretch in the prevention of serial sarcomere loss in immobilized muscle, " Annals of the Rheumatic Disease, pp. 316-317, 1990

[4] M. GIRONE, "A stewart platform-based system for ankle telerehabilitation, " Autonomous Robots 10, pp. 203-212, 2011

[5] M. Boiro, "A new concept of parallel robot for rehabilitation and fitness: the Lambda, " IEEE international conference on Robotics and Biomimetics, pp.2503-2508, 2009

[6] H. Toda, T. Matumoto, R. Tanizaki, T. Imaeda, "Ankle joint pushing mechanism by Stabilization of ankle position using a brace structure, Journal of Advanced Mechanical Design Systems and Manufacturing, " Vol. 10, No. 1, pp. 1-11, 2016

[7] Zhou Z, Sun Y, Wang N, Gao F, Wei K and Wang Q"Robot-assisted rehabilitation of ankle plantar flexors spasticity: A 3 month study with proprioceptive neuromuscular facilitatio, " frontiers in Neurorobotics, 2016

[8] K. Tomioka, K. Sakae and J. Yasuda, "Low back Load Reduction Using Mechanical Lift during Transfer of Patients -A Validation Study Designed to the Acquired Skill for Caregivers, " Sangyo EiseigakuZassi, pp. 103-111, 2008

[9] K. Iwasaki, M Takahashi, M, Sotoyama, X. Liu and A. Koda, "Low back pain among workers in care facilities for elderly after introducing welfare equipment, Sangyo EiseigakuZassi, " pp. 130-142, 2016

Instructions for Authors

Essentials for Publishing in this Journal

1 Submitted articles should not have been previously published or be currently under consideration for publication elsewhere.

2 Conference papers may only be submitted if the paper has been completely re-written (taken to mean more than 50%) and the author has cleared any necessary permission with the copyright owner if it has been previously copyrighted.

3 All our articles are refereed through a double-blind process.

4 All authors must declare they have read and agreed to the content of the submitted article and must sign a declaration correspond to the originality of the article.

Submission Process

All articles for this journal must be submitted using our online submissions system. http://enrichedpub.com/ . Please use the Submit Your Article link in the Author Service area.

Manuscript Guidelines

The instructions to authors about the article preparation for publication in the Manuscripts are submitted online, through the e-Ur (Electronic editing) system, developed by **Enriched Publications Pvt. Ltd**. The article should contain the abstract with keywords, introduction, body, conclusion, references and the summary in English language (without heading and subheading enumeration). The article length should not exceed 16 pages of A4 paper format.

Title

The title should be informative. It is in both Journal's and author's best interest to use terms suitable. For indexing and word search. If there are no such terms in the title, the author is strongly advised to add a subtitle. The title should be given in English as well. The titles precede the abstract and the summary in an appropriate language.

Letterhead Title

The letterhead title is given at a top of each page for easier identification of article copies in an Electronic form in particular. It contains the author's surname and first name initial .article title, journal title and collation (year, volume, and issue, first and last page). The journal and article titles can be given in a shortened form.

Author's Name

Full name(s) of author(s) should be used. It is advisable to give the middle initial. Names are given in their original form.

Contact Details

The postal address or the e-mail address of the author (usually of the first one if there are more Authors) is given in the footnote at the bottom of the first page.

Type of Articles

Classification of articles is a duty of the editorial staff and is of special importance. Referees and the members of the editorial staff, or section editors, can propose a category, but the editor-in-chief has the sole responsibility for their classification. Journal articles are classified as follows:

Scientific articles:

1. Original scientific paper (giving the previously unpublished results of the author's own research based on management methods).
2. Survey paper (giving an original, detailed and critical view of a research problem or an area to which the author has made a contribution visible through his self-citation);
3. Short or preliminary communication (original management paper of full format but of a smaller extent or of a preliminary character);
4. Scientific critique or forum (discussion on a particular scientific topic, based exclusively on management argumentation) and commentaries. Exceptionally, in particular areas, a scientific paper in the Journal can be in a form of a monograph or a critical edition of scientific data (historical, archival, lexicographic, bibliographic, data survey, etc.) which were unknown or hardly accessible for scientific research.

Professional articles:

1. Professional paper (contribution offering experience useful for improvement of professional practice but not necessarily based on scientific methods);
2. Informative contribution (editorial, commentary, etc.);
3. Review (of a book, software, case study, scientific event, etc.)

Language

The article should be in English. The grammar and style of the article should be of good quality. The systematized text should be without abbreviations (except standard ones). All measurements must be in SI units. The sequence of formulae is denoted in Arabic numerals in parentheses on the right-hand side.

Abstract and Summary

An abstract is a concise informative presentation of the article content for fast and accurate Evaluation of its relevance. It is both in the Editorial Office's and the author's best interest for an abstract to contain terms often used for indexing and article search. The abstract describes the purpose of the study and the methods, outlines the findings and state the conclusions. A 100- to 250-Word abstract should be placed between the title and the keywords with the body text to follow. Besides an abstract are advised to have a summary in English, at the end of the article, after the Reference list. The summary should be structured and long up to 1/10 of the article length (it is more extensive than the abstract).

Keywords

Keywords are terms or phrases showing adequately the article content for indexing and search purposes. They should be allocated heaving in mind widely accepted international sources (index, dictionary or thesaurus), such as the Web of Science keyword list for science in general. The higher their usage frequency is the better. Up to 10 keywords immediately follow the abstract and the summary, in respective languages.

Acknowledgements

The name and the number of the project or programmed within which the article was realized is given in a separate note at the bottom of the first page together with the name of the institution which financially supported the project or programmed.

Tables and Illustrations

All the captions should be in the original language as well as in English, together with the texts in illustrations if possible. Tables are typed in the same style as the text and are denoted by numerals at the top. Photographs and drawings, placed appropriately in the text, should be clear, precise and suitable for reproduction. Drawings should be created in Word or Corel.

Citation in the Text

Citation in the text must be uniform. When citing references in the text, use the reference number set in square brackets from the Reference list at the end of the article.

Footnotes

Footnotes are given at the bottom of the page with the text they refer to. They can contain less relevant details, additional explanations or used sources (e.g. scientific material, manuals). They cannot replace the cited literature.
The article should be accompanied with a cover letter with the information about the author(s): surname, middle initial, first name, and citizen personal number, rank, title, e-mail address, and affiliation address, home address including municipality, phone number in the office and at home (or a mobile phone number). The cover letter should state the type of the article and tell which illustrations are original and which are not.

<u>**Address of the Editorial Office:**</u>

Enriched Publications Pvt. Ltd.
S-9,IInd FLOOR, MLU POCKET,
MANISH ABHINAV PLAZA-II, ABOVE FEDERAL BANK,
PLOT NO-5, SECTOR -5, DWARKA, NEW DELHI, INDIA-110075,
PHONE: - + (91)-(11)-45525005

Note